This is to certify that the

thesis entitled

Faulting in an Extensional Environment: An Emplacement Mechanism for the Little Cottonwood Stock, Central Wasatch Mountains, Utah
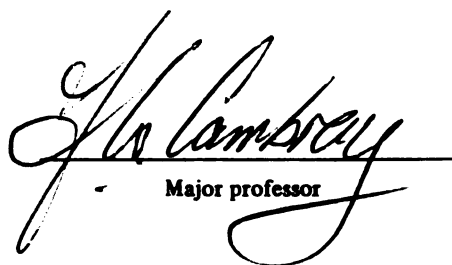
presented by

David W. Szymanski

has been accepted towards fulfillment
of the requirements for

_____M.S._____ degree in __Geology__

_____
Major professor

Date_2/10/99_____

PLACE IN RETURN BOX to remove this checkout from your record.
TO AVOID FINES return on or before date due.
MAY BE RECALLED with earlier due date if requested.

DATE DUE	DATE DUE	DATE DUE

FAULTING IN AN EXTENSIONAL ENVIRONMENT: AN EMPLACEMENT MECHANISM FOR THE LITTLE COTTONWOOD STOCK, CENTRAL WASATCH MOUNTAINS, UTAH

By

David W. Szymanski

A THESIS

Submitted to
Michigan State University
In partial fulfillment of the requirements
For the degree of

MASTER OF SCIENCE

Department of Geological Sciences

1999

FAULTING D
MECHANI

The Little (

:hat is the larges

The WB was emp

approximately 30-

In the stock, the

exhibit pervasive i

Evidence fo

shear zone locate

overlying Mississi

support shearing o

emplacement. Dik

within a releasing

trending northeast-

Emplacement may

to westward cordill

ABSTRACT

FAULTING IN AN EXTENSIONAL ENVIRONMENT: AN EMPLACEMENT MECHANISM FOR THE LITTLE COTTONWOOD STOCK, CENTRAL WASATCH MOUNTAINS, UTAH

By

David W. Szymanski

The Little Cottonwood (LC) Stock, located in the Central Wasatch Mountains of Utah, is the largest pluton in the high-K, calc-alkaline Wasatch Igneous Belt (WIB). The WIB was emplaced at the intersection of the Uinta Arch and Sevier orogenic belt approximately 30-40 Ma. Field evidence does not support models of forcible intrusion for the stock; the rectilinear pluton has a weak internal fabric and wallrocks do not exhibit pervasive intrusion-related ductile deformation.

Evidence for faulting as an emplacement mechanism includes an ultramylonitic shear zone located at the faulted roof contact between the LC granodiorite and overlying Mississippian rocks. Structural and geochemical data from the mylonite support shearing of the LC granodiorite near the roof in an east-west direction during emplacement. Dike-fed emplacement occurred in a releasing step on a dip slip fault, within a releasing bend along an east-west trending strike slip fault. A dike swarm trending northeast-southwest supports extension in a northwest-southeast direction. Emplacement may have been contemporaneous with early Cenozoic extension related to westward cordilleran collapse, but the events may not be coupled tectonically.

For Aaron, Lauren, Alyssa, Haley, Jake, and Brianna.

ACKNOWLEDGEMENTS

TABLE OF CONTENTS

LIST OF TABLES

Figure 31.

Figure 32.

Figure 33.

Figure 34

Figure 35

Figure 36

Figure 37.

INTRODUCT

The Problem

Once t

n the Earth's

r structural g

suggest that pl

regions and d

Clemens. 1992

levels or raisi

must result in

Consequently,

mechanisms sh

evaluated base

field MTPs m

transport crust

zones.

Since t

emplacement c

been classified

passively filling

attractive mecha

Marsh, 1982),

upper-crustal le

INTRODUCTION

The Problem of Pluton Emplacement

Once the "heart of the granitization controversy," the problem of making space in the Earth's crust for large volumes of silicic magmas remains a fundamental problem in structural geology and igneous petrology (Marsh, 1982; p. 809). Recent studies suggest that plutons are often emplaced at great distances (20-40 km) from their sources regions and do not incorporate a great deal of the rock which they intrude (e.g. Clemens, 1998). If one excludes the possibility of lowering the Moho at deep crustal levels or raising the Earth's surface at shallower depths, emplacement mechanisms must result in a zero net change in crustal volume (Paterson and Fowler, 1993a). Consequently, Paterson and Fowler (1993a) argue that pluton emplacement mechanisms should be viewed as material transfer processes (MTPs), and should be evaluated based on the amount of material they can accommodate in the crust. Near-field MTPs move wallrock from the immediate pluton aureole while far-field MTPs transport crustal material back toward the source of generation through subduction zones.

Since the early 1900's, a number of mechanisms have been proposed for the emplacement of magmas (Paterson et al., 1991). Historically, these mechanisms have been classified as "forceful" or "passive," either forcibly pushing aside wallrock or passively filling tectonically created cavities in the crust. Although thermodynamically attractive mechanisms like diapirism have been used to explain emplacement of plutons (Marsh, 1982), most recent studies reject models of forcible emplacement at middle- to upper-crustal levels (see Brown, 1994). Diapirism or in-situ ballooning assumes that

1

gace is made

efects of wh

that extend g

ate for plu

estimate that

accommodate

account for

emplacement

However

involve comp

MTPs operat

emphasize t

creation of

compression

1993)

Faults

MTPs (Pater

magmas by c

rate of openi

ultimately tra

networks, ach

emplacement

space is made for the pluton by ductile shortening of adjacent wallrock, the predicted effects of which are: 1.) high strains in a highly deformed aureole, and 2.) lower strains that extend great distances into the wallrock (Cruden, 1988). Based on wallrock strain data for plutons traditionally interpreted as diapirs, Paterson and Fowler (1993a) estimate that at most, 40% of the total space necessary for emplacement can be accommodated by a near-field MTP of ductile flow. In addition to the inability to account for space based wholly on wallrock shortening, direct evidence of diapiric emplacement is tenuous at best (England, 1990).

However, recent work also suggests that most emplacement mechanisms involve components of *both* forceful and passive intrusion (Hutton, 1988) and multiple MTPs operate around the same pluton (Paterson et al, 1991). These studies tend to emphasize the syntectonic nature of granitoid emplacement and specifically, the creation of space for magmas by local dilatation during regional extension or compression (Hutton, 1997; Cambray et al., 1995; Brown, 1994; Karlstrom et al., 1993).

Faults associated with regional extension can act as both near-field and far-field MTPs (Paterson and Fowler, 1993a). Releasing bends along faults create space for magmas by opening tectonic cavities, provided the rate of magma influx parallels the rate of opening (Paterson and Folwer, 1993b). At the same time, crustal material is ultimately transported back to subduction zones through regional and global fault networks, achieving a zero net change in crustal volume. Figure 1 illustrates fault-type emplacement with generic strike slip and dip slip models. Cambray et al. (1995) apply
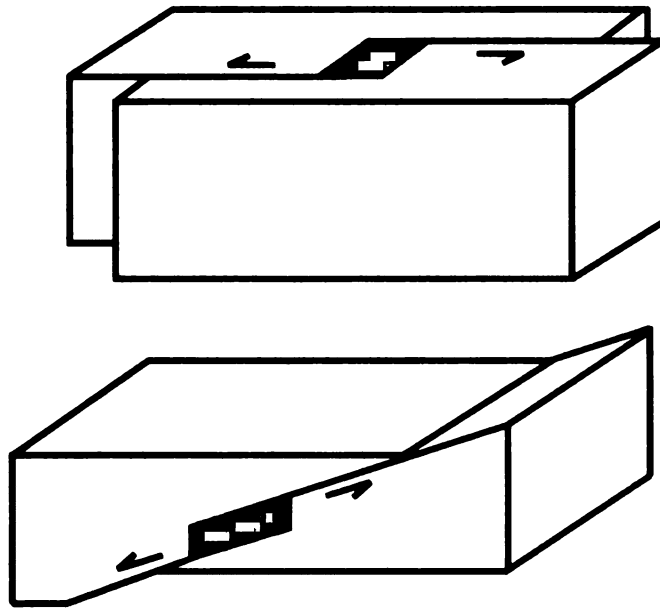
Figure 1.   Simplified block models for fault emplacement. The upper
figure represents a releasing bend along a strike slip fault and
the lower figure illustrates a releasing step on a dip slip fault.
In both figures, the shaded region is magma filling the
tectonic gap created by slip on the fault. Modified from
Cambray et al. (1995).

he terms "releasi

the irregular jogs

slip faults in a nu

Regional Geolog

The Little

suite of high-K, c

Arth in the centr

Kestrey Volcanic

Rocks in the belt

1997, and refere

comprise the coa

eastern porphyri

Valeo, and Pinr

intruded by

accompanied

extensively

districts (Jo

volcanism,

between 30

Crittenden *et*

tilted *the WTB a*

paleodepths for the

in the east (John, 198

the terms "releasing bend" (strike slip faults) and "releasing step" (dip slip faults) for the irregular jogs. Note that models can combine normal or reverse dip slip and strike slip faults in a number of orientations (see Figure 16).

Regional Geology: The Wasatch Igneous Belt (WIB)

The Little Cottonwood Stock is the largest pluton in the east-northeast trending suite of high-K, calc-alkaline stocks exposed along the western extension of the Uinta Arch in the central Wasatch Mountains of Utah (Figure 2). Eleven plutons and the Keetley Volcanics comprise the Wasatch Igneous Belt (WIB) of Vogel et al. (1997). Rocks in the belt are subdivided geographically based on textures described by John (1997) and references therein. The Little Cottonwood, Alta, and Clayton Peak stocks comprise the coarsely porphyritic to equigranular western group of plutons, while the eastern porphyritic group is comprised of the Flagstaff, Ontario, Mayflower, Glencoe, Valeo, and Pine Creek stocks (Figure 3). Further to the east, the Keetley Volcanics are intruded by the Park Premier Stock and Indian Hollow Plug. Mineralization accompanied emplacement; large deposits of Mo, Cu, Ag, Au, Pb, and Zn have been extensively mined in the Big Cottonwood, Little Cottonwood, and Park City mining districts (John, 1997 and references therein). Emplacement of the stocks and associated volcanism, hydrothermal alteration, and mineralization occurred in the mid-Tertiary between 30 and 40 Ma (John et al., 1997; Vogel et al., 1997; Bromfield et al., 1977; Crittenden et al., 1973). Post-emplacement late Cenozoic Basin and Range extension tilted the WIB approximately 15 degrees to the east (John, 1997). Presently exposed paleodepths for the plutons range from ~11 km on the western edge of the belt to <1 km on the east (John, 1989).
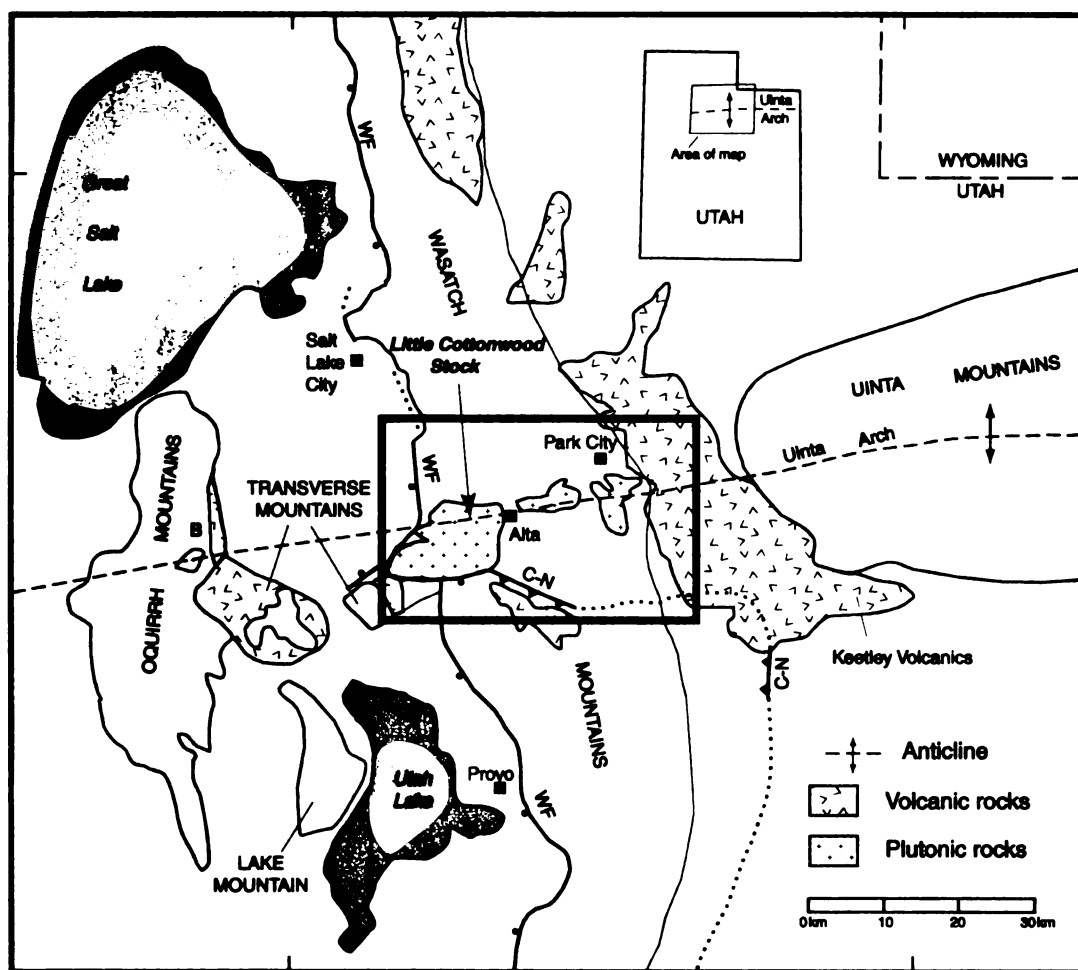
Figure 2. Location map for the Wasatch Igneous Belt (WIB) and the Little Cottonwood
Stock. The dark box (area in Figure 3) encloses the 11 stocks in the WIB and
the westernmost portion of the Keetley volcanics. WF = Wasatch Fault,
C-N = Charleston-Nebo thrust fault. Modified from John (1997).
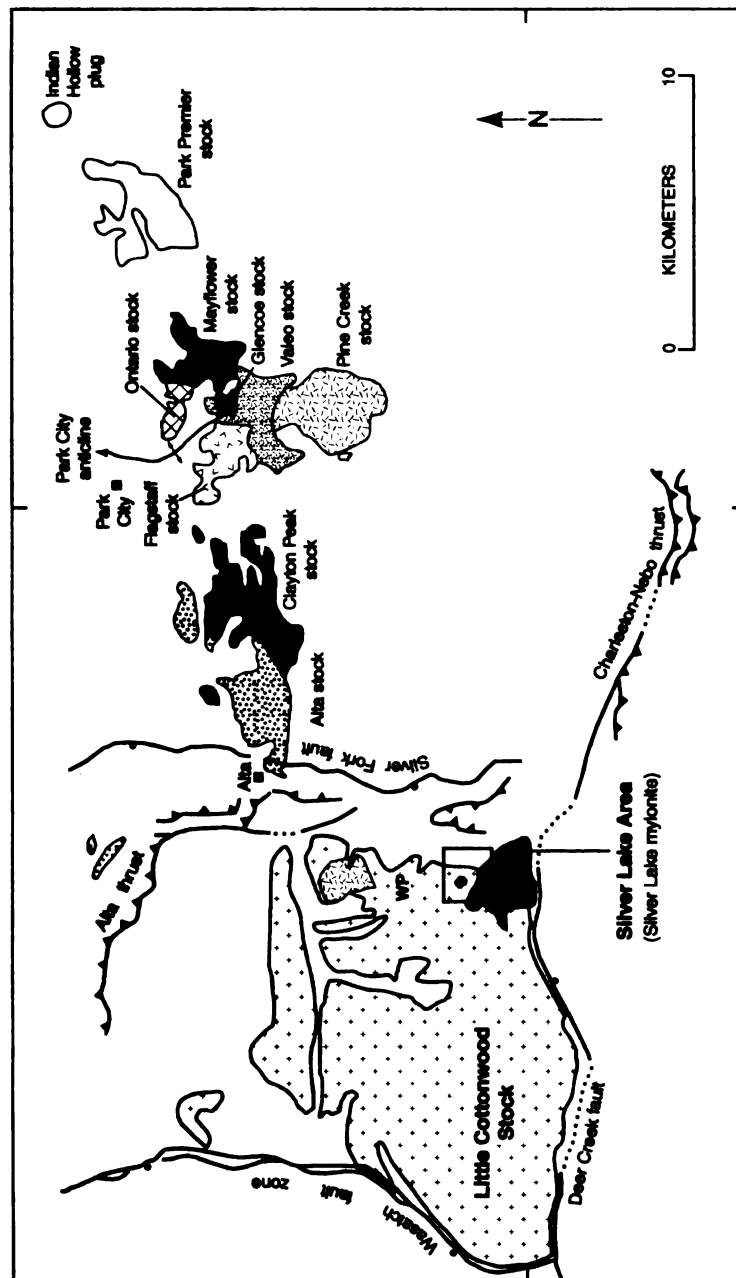
Figure 3. Close-up of the WIB plutons from Figure 2, including the Little Cottonwood Stock. Note the location of the Silver Lake area near the southeast margin of the pluton. The Silver Lake mylonite is located at the contact between the Little Cottonwood granodiorite (LC) and Doughnut Formation (Mdo). A portion of the boxed area is shown in both Figure 4 and Figure 5. WP = White Pine Intrusion. Modified from John (1997).

The Wasatch Mountain Range trends north from central Utah into the southeastern corner of Idaho. The range is the result of a complex tectonic history, recorded in well-exposed late Proterozoic to late Mesozoic sedimentary and metasedimentary units. The range is dominated by structures formed by late Mesozoic Sevier folding and thrusting and periods of Cenozoic extension (Presnell, 1997; John, 1989). The WIB resides within the Cottonwood metamorphic core complex (new name, Constenius, 1998) and is located at the intersection of the Uinta Arch and the Sevier orogenic belt, west of the Colorado Plateau. Intrusion of the WIB clearly postdates the Sevier phase of the Cordilleran orogeny as the plutons cross-cut Sevier thrust sheets. Parallel to the Uinta Arch, a crustal suture separates Archean rocks to the north from Proterozoic to the south, and is the first-order structural control on the emplacement of the WIB (Presnell, 1997). The Wasatch fault (see Figure 2) forms the westernmost boundary of the central range and represents the easternmost extent of the Neogene Basin and Range Province. During the Paleogene, a decreased rate of convergence between the North American and Pacific plates and steepening of the angle of subduction initiated regional extension (see Wernicke, 1992 and references therein). As intraplate compressional stresses were reduced the gravitationally unstable cordilleran wedge spread laterally (Coney and Harms, 1984). The westward collapse was at least partially accommodated by detachments that took advantage of pre-existing Sevier thrust structures (Constenius, 1998). Tertiary dikes pervade the region (Vogel et al., 1997). The dikes have similar ages (30-40 Ma) and chemical compositions to their associated plutons. Overall, the dikes have a northeast-southwest trend, indicating a maximum extension direction oriented northwest-southeast (see inset map, Figure 16).

7

Locate

Cottonwood S

Lawton, 198

classifications

LC granodi

eastern sides

the west and

northern mar

Deer Creek f

Charleston-N

Rece

stock of 30.9

for biotite

metasedime

quartzites a

side of the

carbonate u

margin of

(Mdo) car

Approxim

section (C

fault (new

Located on western edge of the central Wasatch range (Figure 3), the Little Cottonwood Stock has a rectilinear exposure over an area of approximately 115 km^2 (Lawton, 1980). Although various modal analyses have led to different lithological classifications of the Little Cottonwood, it is referred to here as the Little Cottonwood (LC) granodiorite. Intrusive contacts are preserved on the northern, western, and eastern sides of the stock (Lawton, 1980). The pluton is bound by the Wasatch fault to the west and by the Deer Creek fault to the south. The Deer Creek Fault forms the northern margin of the Charleston-Nebo thrust sheet. Constenius (1998) interprets the Deer Creek fault as a reactivated sole fault associated with westward movement of the Charleston-Nebo (C-N) allochthon during the Paleogene-Neogene cordilleran collapse.

Recent U/Pb zircon dating yields an emplacement age for the Little Cottonwood stock of 30.5 $\pm$ 0.5 Ma (Vogel et al., 1997). This date is consistent with $^{40}Ar/^{39}Ar$ dates for biotite and K-feldspar samples. The stock intrudes autochthonous Proterzoic metasediments of the Big Cottonwood Formation (pЄbc), consisting of interbedded quartzites and shale/siltstone units (Lawton, 1980; Crittenden, 1965). On the eastern side of the pluton, sequences of middle Cambrian to lower Mississippian clastic and carbonate units are repeated by complex faulting (Crittenden, 1965). Near the southeast margin of the Little Cottonwood, a section of Mississippian Doughnut Formation (Mdo) carbonates is located on top of the stock near the Silver Lake area (Figure 3). Approximately 800-1000 m of lower Mississippian carbonates are missing from the section (Crittenden, 1965). The section was removed by the Silver Lake detachment fault (new name, Constenius, 1998), which has a normal sense of displacement. The

8

rahment is

Cerstenius (19

Near t

southwest dip

area in Figure

ids formed

mylonite (nev

of a block of

seen in a pho

1:240 scale

are given in

shows the de

Silver Lake m

Previous Wo

Lawto

of the LC g

structure of t

are cross-cut

contacts tend

are concorda

was vertical.

Cottonwood

concordant w

detachment is part of the tectonically reactivated Alta thrust zone described by Constenius (1998).

Near the LC/Mdo contact on the west wall of the Silver Lake Cirque, a west-southwest dipping mylonitic shear zone is exposed within the granodiorite (see boxed area in Figure 3). The exposure was initially identified as a shear zone by tight sheath folds formed in a narrow zone of extremely fine-grained rocks. The Silver Lake mylonite (new name, Constenius, 1998) is located near the LC/Mdo contact, at the base of a block of Mdo which was dropped down by a normal fault. The faulted contact is seen in a photo mosaic of the west wall of the cirque (Figure 4). A corresponding 1:2400 scale map was produced for the west wall (Figure 5); details of field methods are given in Appendix A and a full description of the area is given below. The map shows the detachment-faulted LC/Mdo contact of Constenius (1998) and adjacent Silver Lake mylonite near the tip of the down-dropped Mdo block.

Previous Work on the Little Cottonwood Stock

Lawton (1980) provides a detailed description of the structure and petrography of the LC granodiorite and adjacent wallrocks. With regard to the overall contact structure of the pluton, Lawton (1980) notes the following. 1.) Although local contacts are cross-cut by dikes and the pluton is riddled with wallrock xenoliths in some areas, contacts tend to be sharp rather than gradational. 2.) Planar flow structures (schlieren) are concordant with pluton contacts and steeply dipping, suggesting that magma flow was vertical. 3.) The northern contact between the Little Cottonwood and Big Cottonwood Formation is discordant, while the western and eastern contacts are concordant with bedding. Lawton (1980) attributes the concordant western contact to

9
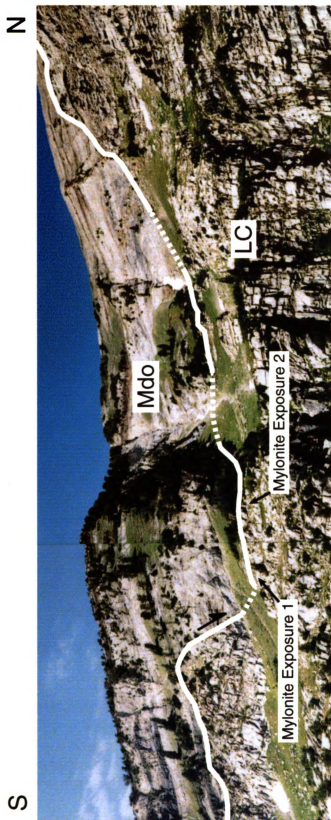
Figure 4. Photo mosaic of the west wall in the Silver Lake cirque. Note the contact between the Little Cottonwood (LC) granodiorite (LC) and Doughnut Formation (Mdo) roof rocks. Exposed contact is solid while inferred contacts are dashed. The approximate location of the two mylonite exposures are marked along the contact. Also note the normal fault that dropped down the mylonite at the base of the contact. The area in the photo corresponds to the map in Figure 5.

10
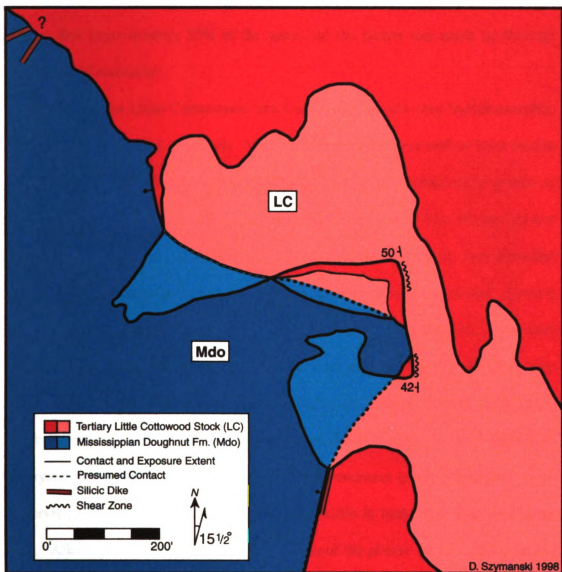
Figure 5. Map showing the contact between the Little Cottonwood grandodiorite
(LC) and Doughnut Formation (Mdo) in the Silver Lake area. Darker
shades represent exposures while lighter shades represent inferred
lithologies. Location of the map area can be found on Figure 3 and seen
in the photo mosaic in Figure 4.

11

the flow of hotter, more ductile wallrocks, which is supported by the presence of higher-grade metamorphic assemblages. On the eastern side, the stock may have intruded along bedding planes. Based on the deflection of marker beds, Lawton (1980) estimates that approximately 33% of the space for the pluton was made by forceful displacement of wallrocks.

Rocks of the Little Cottonwood Stock are white-to-light gray hypidiomorphic, equigranular to porphyritic granitoids. Modal analyses by different authors have lead to classifications of the Little Cottonwood that range from quartz monzonite to granite or granodiorite (see Vogel et al., 1997; Lawton, 1980; Crittenden, 1965). Primary phases include quartz, plagioclase, alkali feldspar, biotite, and hornblende; the most abundant accessory mineral phases are magnetite, sphene, apatite, epidote, and zircon. Lawton (1980) gives a range of plagioclase compositions from An_{30} to An_{20}. Twinned plagioclase crystals exhibit normal or oscillatory zoning patterns and are commonly found as both phenocrysts and groundmass constituents. Large (>2.5 cm) euhedral to subhedral, perthitic alkali feldspar grains represent the most sizeable phenocrysts (i.e. megacrysts) in the pluton and may also occur as groundmass grains. In larger K-spar phenocrysts, albite exsolution lamellae are often visible in both thin section and hand sample. Alkali feldspar phenocrysts in some areas of the pluton are as large as 6.0 cm in length; Figure 6 shows a phenocryst from the Ferguson Canyon area near the northern contact of the pluton (see also John, 1989). Discontinuous schlieren bands and mafic enclaves are found throughout the pluton (Figure 7 and Figure 8). Modal abundances of mafic phases increase in schlieren bands. An intrusion into the Little Cottonwood while it was at least partially crystalline is found in White Pine Canyon, on

Figure 6.   K-Spar megacryst on a weathered LC granodiorite outcrop
in the Furgeson Canyon area, near the northern margin of the
Little Cottonwood Stock.

Figure 7.   Schlieren bands in the Silver Lake area. The surface on
            which the schlieren bands are exposed is nearly horizontal
            and generally planar.

Figure 8.   Mafic Enclave in the Silver Lake area. The long axis length
of this enclave is about average for enclaves measured in the
Silver Lake area.

the eastern side of the pluton. Crittenden (1965) mapped the White Pine intrusion as a leucocratic quartz monzonite.

PURPOSE

The purpose of this study is two-fold. The first part is to describe in detail the structure and geochemistry of the Silver Lake mylonite and determine its relationship to the emplacement of the Little Cottonwood Stock. The second part is to evaluate fault-related emplacement models for the pluton based on the available evidence.

FIELD OBSERVATIONS

Wallrock Deformation

Contacts on the northern, eastern, and southern margins of the pluton were examined for intrusion-related deformation. (Field methods are detailed in Appendix A.) The quartzites and metapelites of the Big Cottonwood Formation on the northern margin of the pluton exhibit both brittle and ductile deformation features, including fault and frictional slide surfaces with mineral lineation (slickensides), small-scale (~ 1.0 m) folding, dislocations and boudinage, rotated porphyroblasts, and small-scale shear zones. Figure 9 is a photograph of a small-scale shear zone in a quartzite interval of the Big Cottonwood Formation. It remains unclear whether these features are associated with the intrusion of the Little Cottonwood Stock, late Mesozoic thrusting during the Sevier phase of the Cordilleran orogeny, or Precambrian deformation.

Large-scale folding and contact metamorphism are found in Mdo carbonates on top of the LC granodiorite on the southeast corner of the pluton. The limestone

16

Figure 9.   Small ductile shear zone in a quartzite interval of the Big
             Cottonwood Formation, located at the northern margin of
             the pluton. The pen in the photo is slightly oblique to the
             trend of the shear zone on the outcrop surface. Below the
             shear zone on the outcrop is a sketch of inferred right
             lateral shear from S-C structures.

protolith has a coarse, sugary texture indicative of recrystallization. Both here and in the wallrock to the north, it is unclear how much, if any of the deformation can be attributed to the intrusion of the Little Cottonwood, as opposed to previous deformation events. The LC/Mdo contact is marked by numerous dikes and sills that interleave LC granodiorite with Mdo wallrock. Coarse- and fine-grained dikes are found both parallel and oblique to the contact, frequently cross-cutting one another and plucking Mdo blocks from the wallrock. In one incidence an angular block (xenolith) of Mdo was observed suspended in a fine-grained LC dike (Figure 10), similar to the wallrock stoping described by Lawton (1980). The strain state of Mdo wallrock is unclear due to poor exposure, inaccesible outcrops, and heavy weathering of the metamorphosed carbonate.

Textural Variation of Intrusive Contact Rocks

For petrographic analysis, 16 oriented thin sections were produced for 11 granodiorite samples collected near pluton contacts in order to look for fabric alignment in the pluton. A detailed description of sampling and field methods is given in Appendix A. Planes for thin sections were measured directly on samples using a goniometer, intersecting planes were plotted and constructed on steronets. Aside from local variation in phenocryst size and abundance of mafic phases, the Little Cottonwood Stock is texturally and mineralogically fairly uniform throughout its exposure (Lawton, 1980). No grain alignment was observed in the samples. Figure 11 is a photomicrograph showing a common equigranular texture in a granodiorite sample taken near the roof pendant contact at Silver Lake cirque, less than 30 cm from the contact. Anhedral to subhedral quartz, plagioclase, and alkali feldspar (microcline)

18

Figure 10. Small fragment of Mississippian Doughnut Formation (Mdo)
wallrock suspended in an LC granodiorite dike near the
faulted roof contact at Silver Lake.

1.0 mm
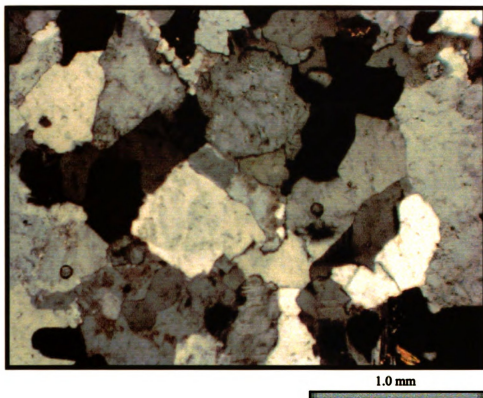
Figure 11. Photomicrograph of LC granodiorite sample 8-97-16 from the Silver Lake area under cross polars. Note that grains of major phases (quartz and feldspars) are generally equidimensional. A small biotite grain is seen in the lower left hand corner.

grains exhibit irregular, weakly serrate grain contacts. Crystals of these major phases are generally equidimensional; average grain size ranges from 0.25 to 1.5 mm. The grain size of the sample shown in Figure 11 is not representative of the pluton as a whole, though Lawton (1980) notes that groundmass grain size sometimes decreases to 1 mm within 10 cm of the contact.

Granodiorite textures at the pluton contacts are variable. Although samples collected near the northern contact exhibit the common equigranular textures described above, several samples taken less than 15 m from the contact show a decrease in average matrix grain size that is interpreted to be a chilled margin texture. For example, Figure 12 shows the quenched texture of a granodiorite sample located approximately 11 m from the contact. Zoned plagioclase phenocrysts (>2.5 mm) are surrounded by a groundmass dominated by fine-grained quartz and feldspar (~0.2 mm). Note the well-developed, though irregular crystal growth fronts where the plagioclase phenocryst and quartz crystals have intergrown, indicating late-stage crystal growth during cooling.

Mafic Enclaves

Numerous studies have used orientation and shape of deformed strain markers in plutons (xenoliths, mafic enclaves) as evidence of emplacement type (e.g. Ramsay, 1989). This assumes that randomly oriented spherical or ellipsoidal enclaves in a partially crystalline magma body will develop preferred shapes and orientations as subsequent pulses of magma flow into a chamber and expand outward. Flattening strains derived from oriented enclaves at pluton margins are often offered as support for diapiric emplacement or in-situ pluton ballooning (see Cruden, 1990 and references

21

1.0 mm
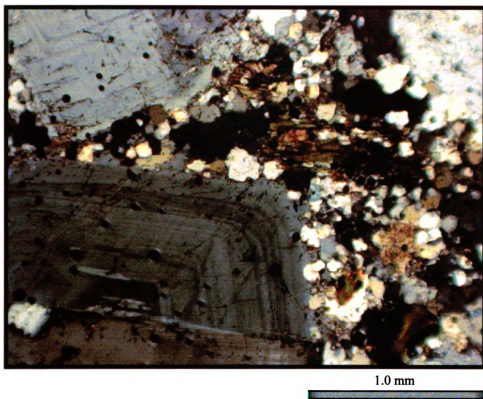
Figure 12. Photomicrograph of granodiorite sample 080597-05 under cross polars. Note the contact between the large euhedral plagiogclase crystal and smaller matrix grains.

therein). Hutton (1988) predicts non-concentric patterns of contact-parallel flattening strains recorded by markers during faulted-related emplacement. The timing relationships for enclave formation and internal emplacement-related deformation of plutons are poorly understood. Enclaves may not be truly passive markers that record finite strain during emplacement. However, Paterson et al. (1991) cite the usefulness of enclaves as qualitative strain data.

In the Silver Lake area, long axis orientations of twenty-nine mafic enclaves in the Little Cottonwood Stock were measured on horizontal planes. Lengths of long and short axes were measured for each enclave. Figure 8 shows a typical spheroidal enclave exposed in two dimensions. Long axes are typically < 13.0 cm; the largest measured long axis was 32.8 cm. Summary data for enclaves are given in Table 1, Appendix B.

A pie type bidirectional rose diagram (Figure 13) was produced for enclave long axis orientations (n=29) using Stereonet Version 3.0 for Windows (Steinsund, 1995). The stereonet was divided into thirty-six sectors, 10° per sector, and pie slices were scaled to fit the largest population sector on the diagram. Raw measurements for enclaves are included in Table 1. The small data set shows several larger populations trending roughly north-south, with the mean orientation calculated as 183° or 003°.

Final long-to-short axis ratios (R_f) were plotted against enclave orientation with respect to north (ϕ'), based on the R_f/ϕ' method for determining strain (Ramsay and Huber, 1983). Figure 14 shows the R_f/ϕ' plot for enclave measurements in this study. R_f defines the deformed shape of an initially spherical or ellipsoidal object in two
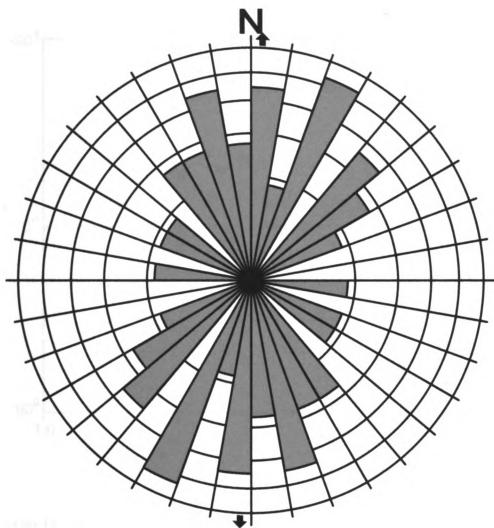
Figure 13. Bidirectional pie type rose diagram for mafic enclaves
(n=29) in the Silver Lake area. Note that there are 36
10 degree divisions and the ring scale is logarithmic.
The arrow displays a mean enclave orientation of
183° (or 003°).
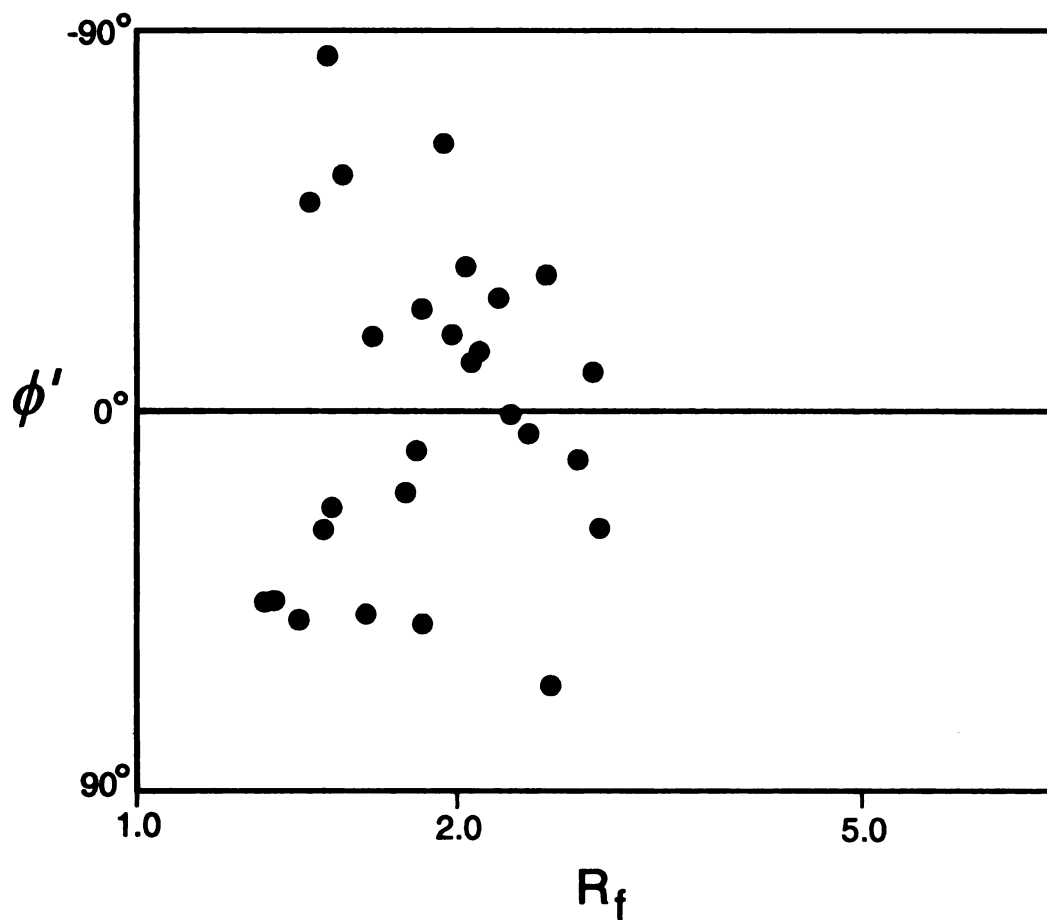
Figure 14. Rf/ϕ' plot for mafic enclaves in the Silver Lake area, where Rf is the final long axis/short axis ratio and ϕ' is the orientation of the long axis with respect to north. Note that the scale for Rf measurements on the x-axis is logarithmic based on the method described by Ramsay and Huber (1983).

dimensions and ϕ' is the orientation of the deformed marker to an initial reference direction (Ramsay and Huber, 1983). The ellipticity, R, of an object is given by

$$R = (1+e_1)/(1+e_2). \qquad\qquad \text{eq. (1)}$$

Assuming the enclaves were all initially spherical, their final shapes and orientations are the result of a superimposed strain ellipse. The superimposed strain ellipse is extrapolated from the data by comparing the R_f/ϕ' plot to a set of reference curves. However, a reliable fit to a standard reference curve for strain ellipticity could not be made with confidence. The data set for enclaves may be a poor representation of strain in the Silver Lake area for several reasons. 1.) The data set may be too small to show strain ratios in a heterogeneous strain field. 2.) Enclaves may not have been initially spherical or randomly oriented (Ramsay and Huber, 1983). 3.) Rheological states and timing relationships between enclave formation and deformation are unknown (Cruden, 1990), therefore enclaves may not record finite strain associated with emplacement of the pluton.

EMPLACEMENT MECHANISM

Synthesis of Evidence for an Emplacement Mechanism

Based on these observations, intrusive contact relationships do not support a large component of forceful intrusion (i.e. diapirism or in-situ ballooning) for the emplacement of the Little Cottonwood Stock. In map view, the Little Cottonwood Stock has a rectilinear shape, not the circular or ovoid shape associated with diapirs or ballooned plutons. Although igneous flow textures (schlieren bands seen in figure 7) are found parallel to linear pluton-wallrock contacts, the generally weak internal fabric does not suggest diapiric emplacement (Vogel et al., 1997). No concentric foliation

26

developed within the pluton or its margins. The shapes and orientations of mafic enclaves do not support forceful emplacement. Contacts are dominantly sharp, not gradational (Figure 15) and chilled granodiorite samples are found at contacts in addition to the equigranular and porphyryritic textures common to the interior of the pluton. Chilled margin textures support intrusion into cold country rock (i.e. tectonically created cavity), not a thermally softened aureole associated with forcible intrusion.

Proterozoic and Mississippian metasediments in contact with the Little Cottonwood have been deformed, but it is not clear that this deformation is intrusion-related. However, even if wallrock deformation is entirely a result of emplacement, balancing the volumetric gain in the crust with the emplacement of the stock by shouldering aside wallrock is impossible. The estimate of a maximum 33% space gain by the forcible sideward displacement of country rock around the Little Cottonwood (Lawton, 1980) is within the 40% maximum estimate of Paterson and Fowler (1993a). Given the lack of pervasive ductile deformation (e.g. tight folding) in the wallrocks, 33% is a generous estimate. As a result, diapirism alone can not be a plausible emplacement mechanism for the Little Cottonwood Stock.

Field relationships support a model of emplacement along a releasing bend or step for the Little Cottonwood. However, in addition to "passive" emplacement along a fault, an additional component of forceful intrusion could help balance the rate of material transfer (tectonic opening) with the rate of magma influx (e.g. Hutton, 1988). Vogel et al. (1997) propose faulting as a far-field MTP for the Little Cottonwood Stock.

27

Figure 15. Sharp contact between LC granodiorite (lower portion of
photograph) and quartzite of Big Cottonwood Formation
at the northern margin of the pluton.

In addition to the volume of space made by shouldering aside of wallrock (a near-field MTP), a model of passive emplacement in a releasing step or bend is invoked to account for at least part of the remaining space required. They cite the following as preliminary evidence in support of a fault emplacement model: 1.) the overall rectilinear shape to the pluton, 2.) the swarm of northeast trending dikes indicating regional extension in a northwest-southeast direction, and 3.) the Silver Lake mylonite associated with the roof contact.

Emplacement Models

Based on the available evidence and regional tectonic framework, this study focuses on two general emplacement models. The first is a simple composite of the generalized releasing step and bend models in Figure 1. In the Vogel et al. (1997) model, a tectonic cavity opens along a west-dipping normal fault within a releasing bend along a left-lateral strike slip fault trending east-west (Figure 16). This model is in agreement with an overall northwest-southeast extension direction required for emplacement of the dike swarm, and predicts shearing along the roof contact during emplacement. A second general model is based on evidence of early Cenozoic extension (Constenius, 1998; 1996). In this case, extension occurs as a result of west-southwest collapse of the cordillera beginning in the Eocene (Constenius, 1996). East-west extension here is also consistent with a dip slip model that predicts shearing at the roof contact during emplacement. However, the left-lateral strike slip fault (Vogel et al., 1997) conflicts with this model. Constenius (1998) suggests the faulted LC/Mdo contact described in "Regional Geology: The Wasatch Igneous Belt (WIB)" is the upper detachment surface which accommodates east-west or even southerly extension.

Map View

Exaggerated regional dike swarm

Wasatch Fault

Little Cottonwood
Stock

Mdo

N

0   KM   10

LC Stock
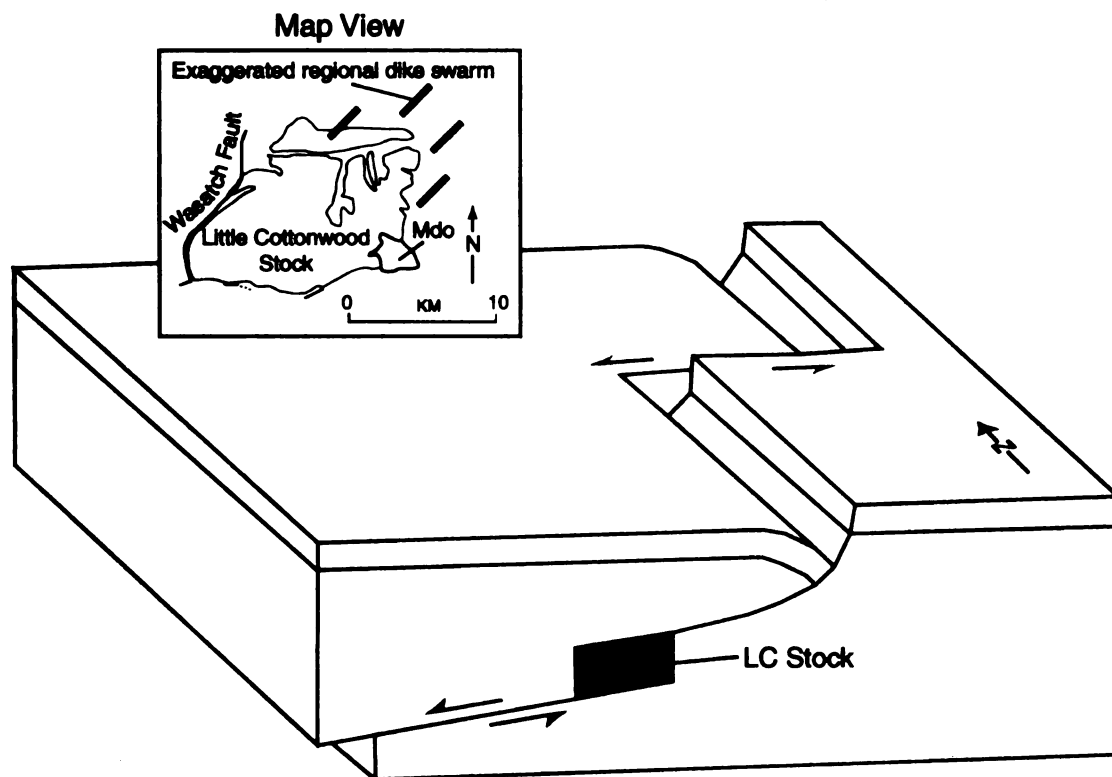
Figure 16. Composite model for emplacement of the Little Cottonwood Stock, a
releasing step on a west-dipping detachment fault within a left-lateral
strike slip fault. The inset map illustrates the shape of the pluton and the
trend of the regional dike swarm, consistent with the opening direction
in the model. Map view modified after John (1997), block model
modified after Cambray et al. (1995).

30

Regional extension in the Vogel et al. (1997) model is in a northwest-southeast direction. In the Cordilleran collapse model the Silver Lake mylonite was part of the detachment and subsequently dropped into the partially crystalline LC granodiorite as the base of a half-graben seen in Figure 17. The Silver Lake mylonite was abandoned in favor of the new path shown in the diagram (Constenius, 1998).

THE SILVER LAKE MYLONITE

The shear zone located on the west wall of Silver Lake cirque provides an excellent opportunity to constrain extension-related fault emplacement models for the Little Cottonwood Stock. Shear zones are tabular bodies of highly concentrated shear strain, bound by relatively unstrained protolith rocks. As such, a "shear zone is a zone of strain softening" where strain is accommodated by dominantly crystal-plastic deformation, i.e. mylonitization (White et al., 1980; p. 175). In general, shear zone mylonites are the product of strain softening and as such, their generation requires extremely localized shear strain (Christiansen and Pollard, 1997; Simpson, 1983, White et al., 1980). Outside of the narrow, well-defined boundaries of the Silver Lake shear zone, granodiorite samples (e.g. Figure 11) are strain-free. Strongly foliated mylonites often contain kinematic indicators (e.g. sheath folds, rotated prophyroblasts) for determining sense of shear. The location and kinematics of the Silver Lake mylonite support a fault emplacement mechanism. A detailed structural description and interpretation of the shear zone follows. In addition, chemical analyses of shear zone samples are presented in an attempt to constrain the protolith.
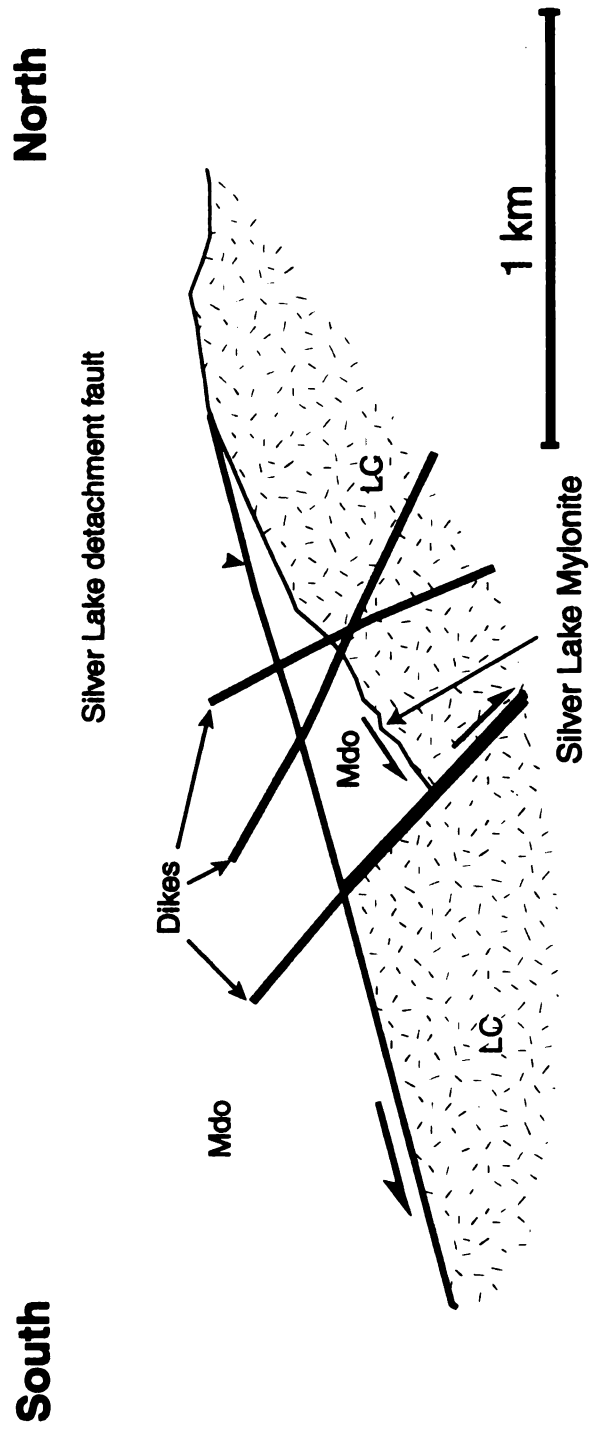
Figure 17. Structural features on the west wall of Silver Lake cirque. Note the down-dropped block of Mdo and the Silver Lake mylonite located at the base of the block. The three aplitic dikes cross cut the half-graben and Silver Lake detachment fault. Modified from Constenius (1998).

Overview and Local Geologic Setting

The shear zone associated with the Silver Lake mylonite is exposed on the west wall of Silver Lake cirque at an elevation of 9400 ft. (See Figure 3 for location of the Silver Lake area and Figure 4 for the location of the shear zone on the wall of the cirque). The outcrop consists of two continuous exposures separated by Quaternary slope talus. The mylonite exhibits mesoscopic foliation planes, deformed by sheath folds but otherwise parallel to shear zone boundaries. As discussed below, in thin section it appears that compositional banding forms the foliation. Fresh surfaces are typically off-white to light green in color; weathered surfaces are light green to brown with rust-brown foliation surfaces. Rocks in the Silver Lake shear zone are completely mylonitized, i.e. all grains underwent size reduction and no porphyoblasts remain in the matrix. Based on the terminology of fault-related rocks outlined by Wise et al. (1984) the Silver Lake mylonite is classified here as an ultramylonite, extensively recrystallized and containing 100% matrix grains typically >>0.1 mm.

Isoclinal or tight recumbent sheath folds identify the tabular rock body as a shear zone. Fine- grained "morphological" mineral lineations form on foliation surfaces and are lithogically indistinguishable from the rest of the rock. The shear zone is always less than 0.5 m wide and has sharp, non-planar boundaries that separate the mylonite from unstrained country rocks. The sharp shear zone boundaries are seen in Figure 18, a photograph of the shear zone, bound on either side by LC granodiorite. The inset diagram in Figure 18 is a schematic field sketch of the shear zone boundaries, drafted normal to the plane of exposure to compensate for the oblique perspective of the photograph and topography on the outcrop. Note the irregular, non-planar nature of the
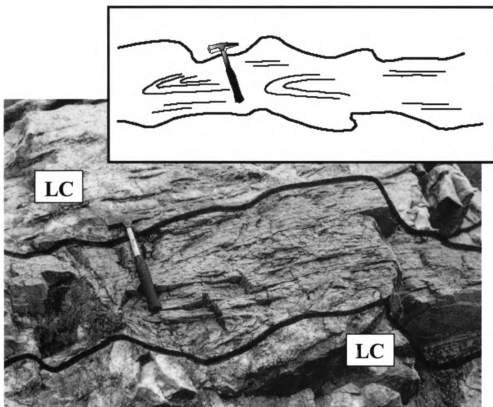
Figure 18. Oblique view of the Silver Lake mylonite. The shear zone in the photograph is outlined in black. Note the sharp contact between the mylonite and unstrained granodiorite protolith. The inset field sketch compensates for the oblique perspective and shows the irregular, non-planar nature of the contact.

granodiorite/mylonite contacts. The shear zone dips moderately (36-50°) and uniformly to the west-southwest (259-266°) along its exposure. As seen on the map in Figure 5, the exposed shear zone is located in the LC granodiorite, close to the LC/Mdo contact. At this location on the west wall of the cirque, the LC/Mdo contact extends down topography (east in map view) as the down-dropped block in Figure 17. An aplitic dike that intrudes the LC granodiorite is truncated by the mylonite.

$^{40}Ar/^{39}Ar$ whole rock dating of the Silver Lake mylonite as reported by Constenius (1998) yields a minimum age of 27.1 ± 0.1 Ma. Additional dates from the same study by Vogel et al. (1997) provide a U/Pb zircon age for the LC granodiorite near the shear zone of 30.5 ± 0.5 Ma. This is in agreement with recent $^{40}Ar/^{39}Ar$ biotite and K-feldspar dating of four LC granodiorite samples from above and below the shear zone. Samples from above the shear zone yield ages of 30.1 ± 0.1 Ma and 30.0 ± 0.1 Ma. Samples from below the shear zone have ages of 30.5 ± 0.1 Ma and 29.7 ± 0.1 (Layer and Damon, pers. comm., 1998). In addition, whole rock $^{40}Ar/^{39}Ar$ dating of the aplitic dike truncated by the mylonite yields an emplacement age of 27.0 ± 0.3 Ma (Vogel et al., 1997).

Mesoscopic Kinematic Indicators: Sheath Folds and Mineral Lineations

In domains of high shear-strain ($\gamma \approx 10$) foliation forms approximately parallel to the flow plane of shear, i.e. shear zone boundaries (Hudleston, 1986; Simpson, 1986). Figure 19 illustrates the formation of foliation during simple shear. A line initially perpendicular to shear zone boundaries will undergo rotation toward the horizontal as ψ increases, where:

$$\gamma = \tan \psi. \qquad \qquad eq. (2)$$
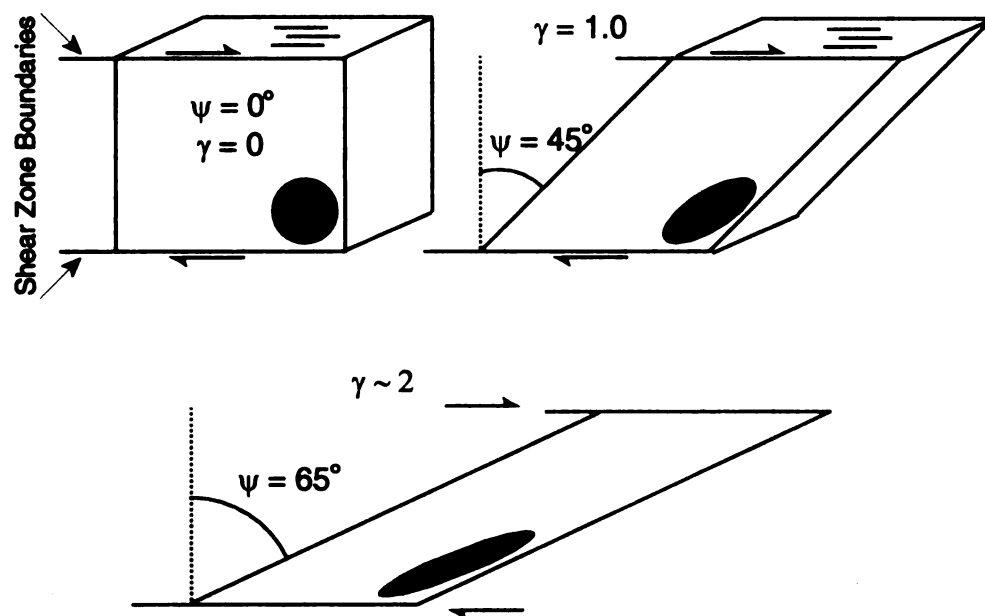
Figure 19. Illustration of foliation development during simple shear. A line
initially perpendicular to the shear zone boundaries will undergo
progressive rotation into parallelism with the boundaries under
high shear strain ($\gamma \sim 10$), by equation (1). Note that the same
diagram explains the rotation of sheath fold axial planes into
parallelism with the shear zone boundaries. The top two blocks
show the orientation of syn-kinematic stretching lineation in the
shear plane during simple shear.

On foliation surfaces, mineral lineations form parallel to the maximum stretch direction. (Similar to the structures described by Christiansen and Pollard (1997), lineations in the Silver Lake mylonite are formed by elongate aggregates of fine-grained material, indistinguishable from the overall rock even in thin section.) Small perturbations in flow, especially in a naturally heterogeneous strain field, can lead to sheath folds in the foliation (Skjernaa, 1989; Hudleston, 1986). The folds often resemble the sheath of a knife with small interlimb angles and curvilinear hinge lines (Ramsay and Huber, 1987; Cobbold and Quinquis, 1980). Sheath folds have been produced in a similar fashion experimentally by Cobbold and Quinquis (1980) by amplifying "initial deflections in an otherwise planar and passive layering which is grossly parallel to the shearing plane" (p. 120). The embayments along the non-planar boundaries of the Silver Lake shear zone suggest that foliation planes developed similar irregularities during shear (Figure 18). These perturbations begin as open, gently doubly-plunging folds within the original foliation. As shear progresses (eq. 1), the hinge line curves symmetrically within the axial surface and the axial surface rotates into parallelism with shear zone boundaries (Figure 19).

Most workers agree that well exposed sheath folds can be used to determine direction and sense of shear, especially when accompanied by corroborating evidence (Crispini and Capponi, 1997; van der Pluijm and Marshak, 1997). The asymmetrical vergence of sheath folds can indicate sense of shear, or the relative displacement (i.e left- or right-lateral) across the shear zone as opposed to a general direction of shearing (Hudleston, 1986). A number of caveats exist for the application of sheath folds as kinematic indicators. The most important caveat is that in the absence of exposed fold

trains across the shear zone, the geometry of a single fold does not yield a unique sense of shear. In addition, symmetry or vergence in non-passive folds (i.e. compositional or rheological buckling or bending) can often yield opposite sense of shear. However, cautious interpretation of shear direction and sense is practical when the initial orientation of foliation in the shear zone is known (Simpson, 1986). In addition, stretching lineation in foliation planes can support interpretation of shear direction when present.

Geometry and Orientation of Sheath Folds and Lineations

Sheath folds in the Silver Lake mylonite are exposed in two, and often three dimensions. Measurements were made on a total of 15 folds across the two shear zone exposures. Table 2 in Appendix B is a list of fold domains and corresponding measurements of axial surfaces and hinge lines. Qualitatively, folds are isoclinal with small interlimb angles (<20°) and variable hinge angles (always estimated <<150°). The folds plot near the Q-R axis between cylindrical isoclines and isoclinal domes on the Williams and Chapman (1979) PQR diagram (Figure 20). From Williams and Chapman (1979), the apexes of the PQR diagram are defined as:

$$P = \alpha/180, \qquad\qquad \text{eq. (3)}$$

$$R = (180 - \beta)/180, \text{ and} \qquad\qquad \text{eq. (4)}$$

$$Q = 180 - (\alpha + (180 - \beta))/180, \qquad\qquad \text{eq. (5)}$$

where α is the interlimb angle and β is hinge angle. Although hinge lines and axial surfaces were measured in three dimensions (see field methods in Appendix A), quantitative classification based on the PQR diagram proves difficult. Figure 21 illustrates the "nose" of a sheath fold in the shear zone. The curvilinear hinge doubly-

planes

P

Silver Lake mylonite sheath folds

cylindrical
isoclines

Q

isoclinal
domes

R

Photo 21   Photo 22
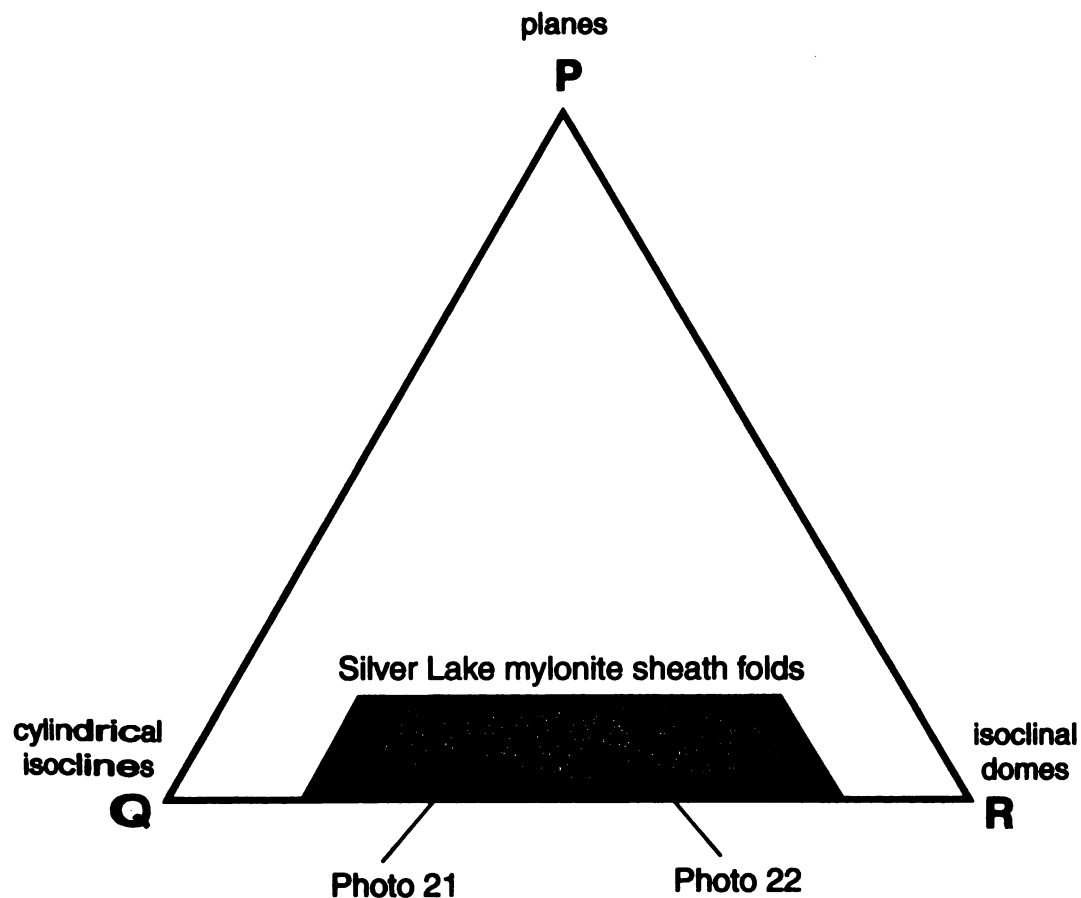
Figure 20. Approximate classification of Silver Lake mylonite sheath folds
based on the Williams and Chapman (1979) PQR diagram. An
explanation for calculation of P, Q, and R values is given in text.
Note that the folds plot close to the Q-R axis, between tight
cylindrical isoclines and tight cylindrical domes. Relative positions
for the folds in Figure 21 and Figure 22 are shown by arrows.

Figure 21. Nose of large sheath fold in the Silver Lake mylonite. The hinge line doubly plunges into a plane normal to the photograph.

plunges obliquely into the plane of the photograph. Although the fold is not fully exposed, a gentle curvature of the hinge can be traced along the nose and the fold plots closer to the "Q" apex on Figure 20. The smaller fold in Figure 22 demonstrates a more curved hinge line, though the oblique three-dimensional profile obscures the extent of the curvature (i.e. the hinge angle, β). Qualitatively, the fold plots closer toward the "R" apex on Figure 20 than the fold in Figure 21.

Figures 23-26 are contoured stereonet projections for fold measurements in the Silver Lake mylonite. All data were plotted and contoured using StereoNet Version 3.0 for Windows (Steinsund, 1995). Contours were produced using a conventional contouring algorithm, measuring distance on the steronet. The density of data points was evaluated using a step function with a standard search radius of 1% of the total area of the lower hemisphere projection. Each time a data point falls within the search area, the value of the counting circle (contoured in percent of total population) increases by one (Steinsund, 1995). The basic step function was chosen for simplicity in contouring relatively small data sets; other contouring methods (e.g. counting by angle on the stereonet) were tested, but did not produce significant variation in contour diagrams.

Contours for poles to axial surface (n=12) show a relatively tight grouping of a single population (Figure 23). The folds are recumbent to gently inclined: axial surface dips range from 9° to 42°. The average axial surface dips shallowly to the west (280°/27°, azimuth). A contour diagram for poles to foliation surfaces shows a grouping similar to axial surface measurements (Figure 24). The average foliation plane (n=20) also dips to the west and has a similar dip amount (288°/31°). Hinge lines are approximately horizontal to moderately plunging, from 3° to 47° and measurements

41

Figure 22.   Small sheath fold in the Silver Lake mylonite.
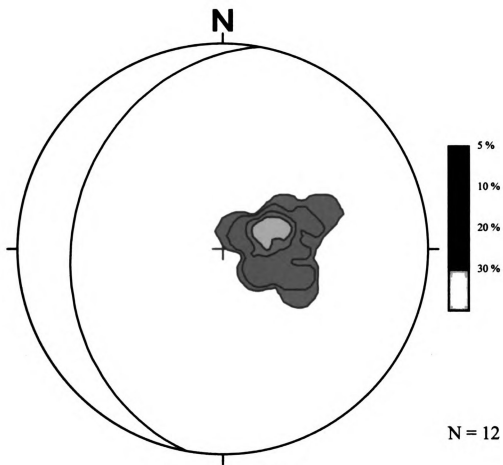
Figure 23. Pole contour diagram for sheath fold axial surfaces in the Silver
Lake mylonite. The great circle represents the average axial
surface (280/27 azimuth).
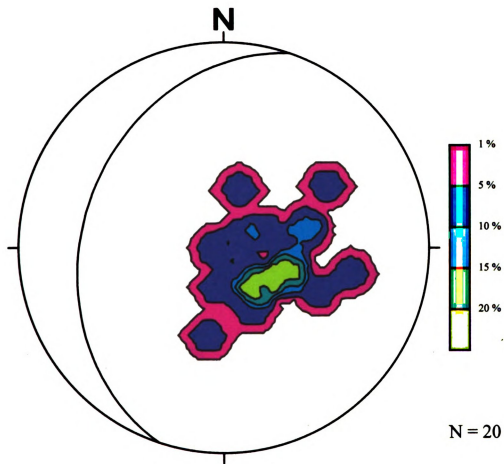
Figure 24. Pole contour diagram for foliation surfaces in the Silver Lake mylonite. The great circle represents the average foliation surface (288/31 azimuth).
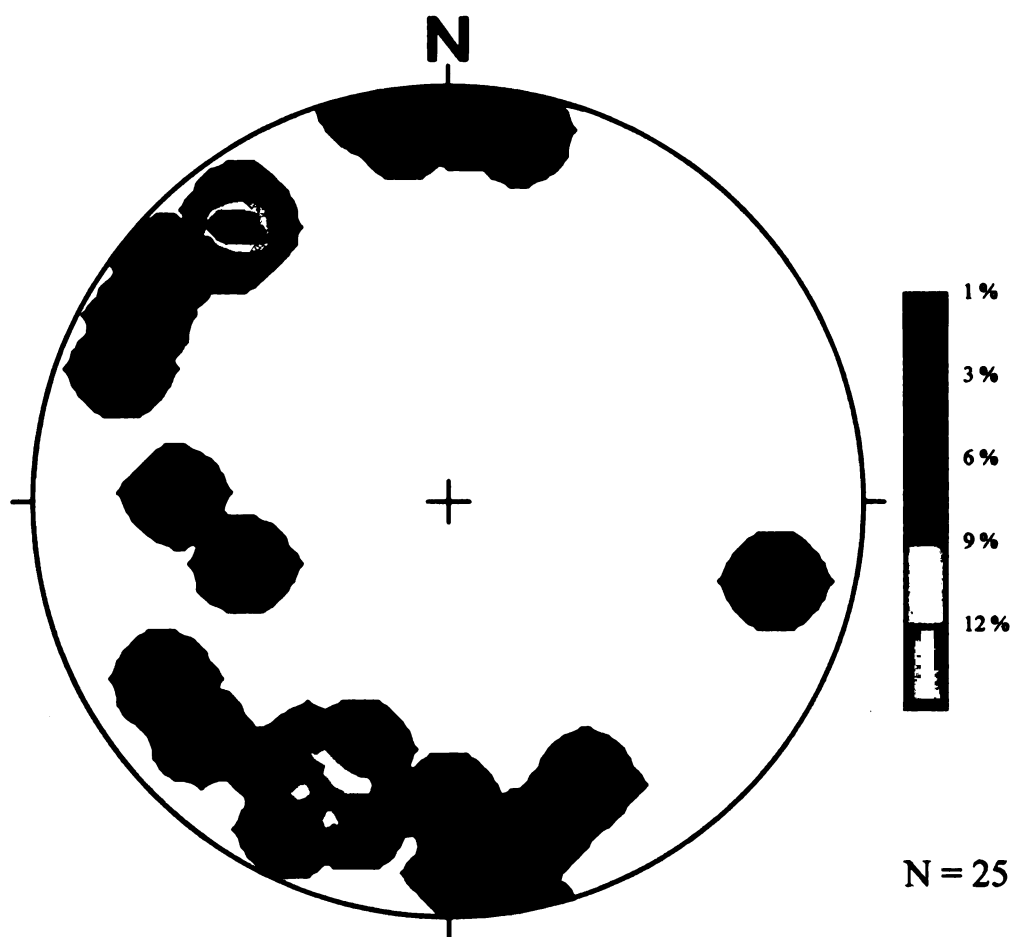
Figure 25. Contour diagram for hinge line measurements on sheath folds
in the Silver Lake mylonite.
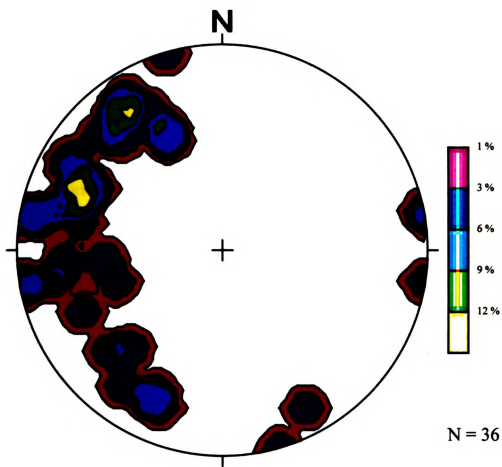
Figure 26. Contour diagram for lineation measurements on foliation surfaces in the Silver Lake mylonite.

(n=25) plot in several populations (Figure 25). The two largest populations plunge to the northwest and southwest, though smaller groups are found plunging to the north and south. One anomalous hinge line is found plunging roughly to the east, contoured as 4% of the total population. Lineations on foliation surfaces (n=36) plot on a west-dipping girdle with several maxima (Figure 26).

Discussion of Sheath Folds and Lineations

Overall, the orientation of sheath folds and stretching lineations in the mylonite support an east-west shear direction. As expected, sheath fold axial surfaces (Figure 23) show similar orientation to foliation in the shear zone (Figure 24). Axial surfaces of sheath folds rotated under high shear strain until subparallel with both foliation and shear zone boundaries. The grossly symmetrical distribution of hinge lines along the average axial surface suggests a population of folds in varying stages of hinge line bending during deformation (Figure 25). Although sheath folds are well exposed, fold trains are not exposed in three-dimensions across the width of the shear zone. As a result, sheath folds in the Silver Lake mylonite do not reveal sense of shear across the zone.

The orientation of lineations offers corroborating, if somewhat peculiar evidence for direction of shear. Assuming a model of simple shear, the aggregates of grains that form strongly lineated fabrics parallel to the stretching direction in the shear plane should show fairly constant orientation across a shear zone (Figure 19). Although flow velocity varies naturally across the zone (responsible for the initiation sheath folds) maximum stretch direction remains in the direction of shear. However, mineral lineations in the Silver Lake mylonite show somewhat more irregular behavior.

47

Lineation measurements lie on the foliation surface as expected (Figure 26). However, they do not plot in one tight group as expected; lineation trend and plunge is not constant within the foliation. In some domains, individual sets of lineations were actually observed to change trend (and consequently plunge) on foliation surfaces. On one foliation surface, individual lineations were observed to be curvilinear, changing trend from 205° to 253° on a foliation plane dipping to 281° (Figure 27). Another foliation plane contains individual lineations ranging in trends from southwest to northwest, in the space of less than 1 m.

The overall radial distribution of lineations and curvature of individual aggregates within axial surfaces (i.e. foliations) suggests that lineations may have pre-kinematic or early syn-kinematic origins and rotated in the shear plane during progressive inhomogeneous deformation. The fan-shaped distribution of lineations plots directly on the average foliation plane. None of the lineations plunge due north or south. Passive linear elements (pre- or early syn-kinematic lineations) on sheath folds would be expected to have a radial distribution about the direction of shear as they rotate within the shear plane. The distribution of lineations on the average axial surface supports an east-west shear direction (Figure 26).

Microscopic Textures of the Silver Lake Mylonite

Using the technique described in "Textural Variation of Intrusive Contact Rocks," 25 oriented thin sections were produced for eight mylonite samples. (In the case of some mylonite samples with partings along foliation surfaces, samples were impregnated with epoxy before final sectioning.) The Silver Lake shear zone is composed of an aphanitic, generally equigranular, quartz-rich ultramylonite. Mylonite
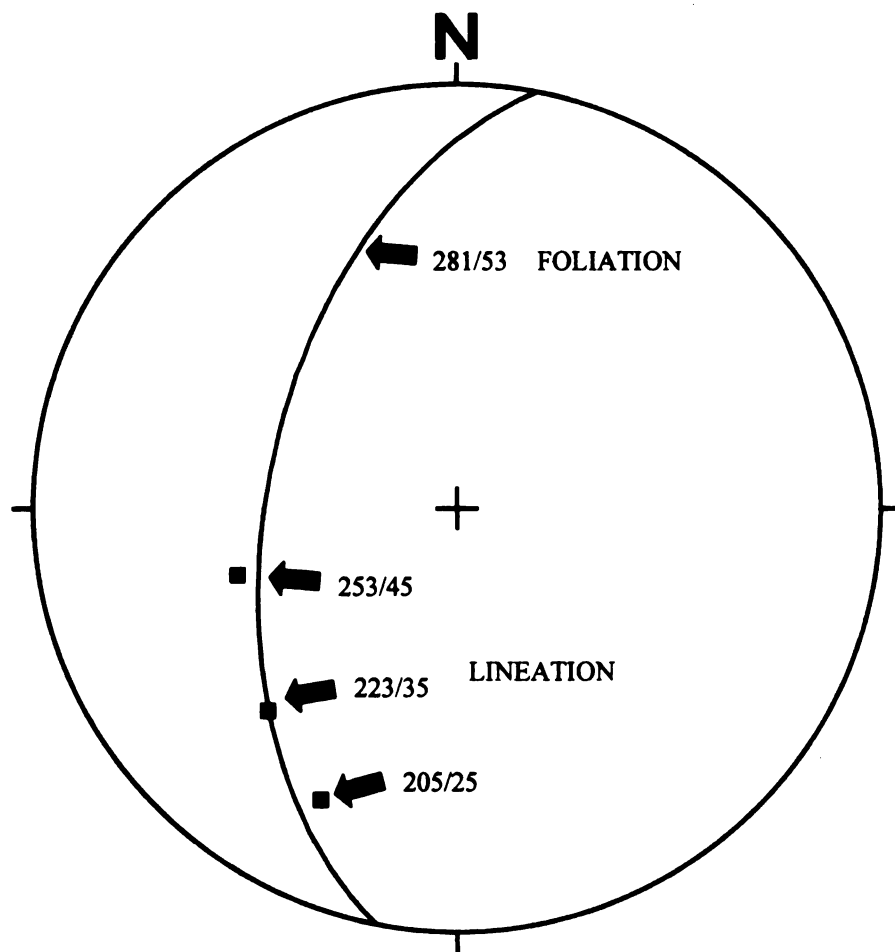
Figure 27. Changing trend and plunge of lineation within a foliation plane.
The great circle is the foliation plane on which measurements
were made. The squares represent three trend and plunge
readings for a single lineation on the surface.

grain size is dramatically smaller than grain size of the Little Cottonwood granodiorite protolith: average grain size of granodiorite samples can be up to 1000 times greater than that of mylonites. The overall texture is similar to commonly described mylonitic textures (Tullis et al., 1982). The presence of a well-developed foliation formed by compositional banding, extremely fine grain size, and microscopic evidence suggests grain size reduction occurred in the Silver Lake samples. As discussed below, grain size reduction was most likely accomplished by crystal-plastic deformation of grains during shear. However, standard microfabric kinematic indicators (see Simpson and Schmid, 1983) are absent in all samples; the ultra fine-grained quartzofeldspathic matrix is porphyroblast-free and lacks oriented fabrics that reveal sense-of-shear. The extremely fine grain size and lack of kinematic indicators most likely resulted from post-shearing (static) recrystallization or annealing.

Petrography

The dominant phases in the Silver Lake mylonite identified in thin section are quartz, plagioclase, alkali feldspar, and white mica. Quartz and feldspar grains are typically equant and extremely fine-grained (>>0.05 mm), where even anomalously large grains are less than 0.5 mm in their longest dimension (Figure 28). The fine grain size makes differentiation between many grains (i.e. feldspar phases) impossible, even under 1000x magnification using a 100x objective oil-immersion lens. However, identification of the most abundant major phases is supported by a CIPW norm calculation for an average mylonite sample that predicts quartz and feldspar as the dominant phases (Table 3 in Appendix C, based on the geochemical analyses made in this study). Similarly, larger grains may have observably sharp grain boundaries, but

1.0 mm
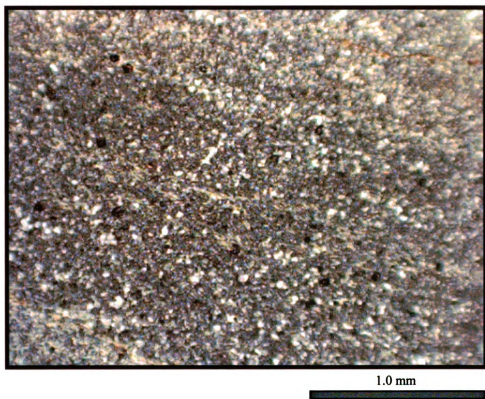
Figure 28. Photomicrograph of mylonite sample 8-97-15 under cross polars. Note the extremely fine grain size of the sample.

most boundaries appear indistinct at limits of resolution and can only be distinguished by patchy, alternating extinction of adjacent grains (Figure 28). Quartz and feldspar grains often form foliation-parallel grain aggregates.

As another primary phase, crystals of white mica display two habits. First, they form individual elongate grains, often oriented parallel or slightly oblique to foliation planes. The grains are typically fine (<0.1 mm) and easily identified using intermediate power (100x) by relief and birefringence under cross-polars. In one sample taken from a sheath fold, mica grains were observed to be slightly oblique to folded foliation planes (Figure 29). Secondly, white micas mantle quartz and feldspar grains, forming an indistinct, colorless, intergranular patchwork fabric (Figure 30). Individual grains appear as ultra fine needle-shaped, grains visible only under high-power (1000x) using a 100x oil immersion objective lens. Aggregates of white mica with this habit occur in bands that define foliation planes parallel to aggregates of quartz and feldspar grains. The micas also mantle the quartz and feldspar grains and exhibit two conjugate preferred orientations approximately 35-45 degrees to foliation planes (Figure 30). Mica grains in each of these orientations go to extinction in unity. Neither orientation is universally dominant when present in a sample.

No accessory phases were identified in thin section, possibly due to the ultra-fine grain size of the mylonite. However, minor oxidation features confirm the presence of small amounts of mafic phases. The only identifiable secondary phase is calcite, appearing as fine-grained patches in a mylonite sample (8-97-17). The presence of carbonate in this sample is confirmed by weak reaction with dilute hydrochloric acid.

1.0 mm
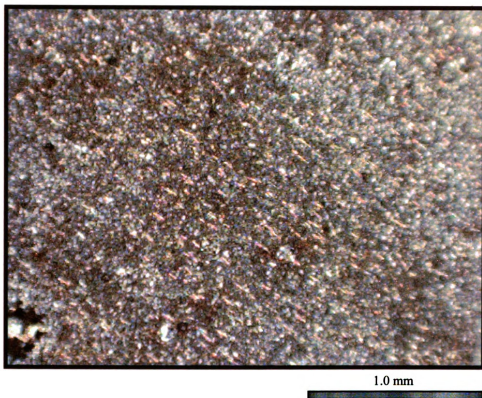
Figure 29. Photomicrograph of mylonite sample 8-97-8 under cross
polars. Note the orientation of fine-grained micas, trending
from the lower right to upper left in the field of view.
The micas are oriented parallel/subparallel to tightly folded
foliation in this sample.

1.0 mm
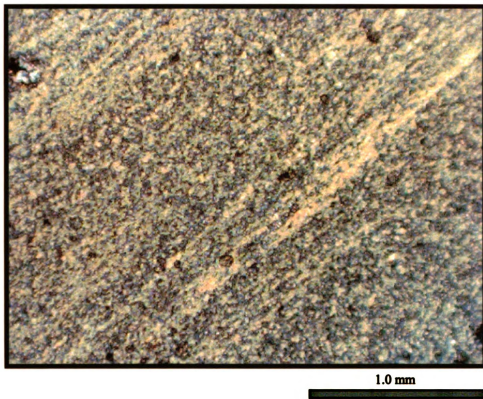
Figure 30. Photomicrograph of mylonite sample 8-97-15 under cross
polars. The light patchwork texture is formed by ultra
fine-grained micas that mantle quartz and feldspar grains.

Microstr

A

foliation

shape pre

with long

made it

without

However

strong LF

C

in shear

and Gapa

the domi

perpetua

develope

(van der

However

sporadica

classic de

microstru

diffusion,

In

presence o

Microstructures

Aggregates of generally equant quartz and feldspar and patchy micas define foliation planes in the Silver Lake mylonite (Figure 28 and Figure 30). No strong grain shape preferred orientation (GSPO) exists, although some quartz and feldspar grains with long axes parallel to foliation planes can be found. The ultra fine-grained textures made it impossible to determine if a lattice preferred orientation (LPO) is present without the use of x-ray goniometry, which was beyond the scope of this study. However, using the gypsum ($\lambda/2$) accessory plate on the polarzing microscope, no strong LPO is evident in thin section scale.

Continuous grain size reduction by dynamic recrystallization is self-propagating in shear zones as strain is accommodated in zones of "runaway instability" (Cobbold and Gapais, 1987). Tullis et al. (1982) note that grain size reduction may even "change the dominant deformation mechanism" to one which further concentrates shear strain, perpetuating the cycle of grain size reduction (p. 230). The fine grain size and well-developed foliation of the Silver Lake mylonite are well known in shear zone rocks (van der Pluijm and Marshak, 1997) and indicative of dynamic recrystallization. However, evidence for individual grain-scale deformation mechanisms is present only sporadically and often equivocal. Hobbs et al. (1976) and Tullis et al. (1982) provide classic descriptions of crystal-plastic deformation mechanisms that produce mylonite microstructures and reduce grain size during ductile shear, including dislocation creep, diffusion, and grain boundary sliding.

In comparison with studies by Simpson (1983) and Tullis et al. (1982), the presence of relatively equant grains with no strong LPO suggests that grain boundary

55

sliding

some Si

angle su

in extinc

the fine

difficult

resolutio

occurred

produced

by elimir

Discussio

Di

for shear

associated

equigranu

indicators

oriented r

several sar

not consist

As

white mica

mylonites (

(S) foliatior

sliding may have partly accommodated strain in the shear zone. Evidence is found in some Silver Lake mylonite samples for subgrain formation and recrystallization. Low-angle subgrain boundaries are evident in quartz grain aggregates, where subgrains vary in extinction by several degrees. Many grains appear strain-free, however, in each case, the fine texture and irregular intergranular patchwork of micas (Figure 30) makes it difficult to discern overall microstructure in the mylonite at thin section-scale resolution. The weak evidence for strain recovery suggests that annealing may have occurred after the removal of shear stress. Some grains preserve miscrostructures produced by dynamic recrystallization while strain-free grains indicate static recovery by elimination of dislocations (Covey-Crump, 1997).

Discussion of Mylonite Microstructures

Due to annealing, the Silver Lake mylonite contains no microscopic evidence for shear sense. Although dynamic recyrstallization occurred, the high temperatures associated with intrusion were superimposed on this dynamic recrystallization. The equigranular quartz-feldspar-mica matrix does not exhibit any standard kinematic indicators: porphyroblasts, rotated pressure shadows, fractured grains, or strongly oriented recrystallized grain fabrics (Simpson, 1983). Thin quartz veins are offset in several samples, but timing relationships cannot be determined and the sense of offset is not consistent in all veins, so they cannot be used as kinematic indicators.

As shown in Figure 30, quartz and feldspar grains mantled by micron-scale white micas in some samples vaguely resemble S-C' structures found in many mylonites (van der Pluijm and Marshak, 1997; Simpson, 1983). The main mylonitic (S) foliation is parallel or subparallel to shear zone boundaries except in fold hinge

regions,

approxii

not inte

The ma

therefore

orientati

unique s

and oppc

T

the mylo

and mylc

differenti

dropped

from the

flattening

may acco

help defir

MYLON

My

for major

evaluate p

that the LC

regions, as seen in outcrop. The two oriented mica textures appear at angles approximately 35-45 degrees to the S foliation. For several reasons, these structures are not interpreted as S-C' structures and cannot provide any kinematic information: 1.) The main mylonitic foliation is parallel or subparallel to shear zone boundaries therefore neither of the two mica "foliations" can be a C-foliation; 2.) If the grain shape orientation were a C'-foliation, displacing the S-foliation, its orientation would yield a unique sense of shear. Instead, textures are oriented in two directions, roughly equal and opposite to that of the main foliation.

The texture formed by the micas suggests that post-shear flattening occurred in the mylonite. Based on the location of the shear zone and age dates for the protolith and mylonite, pure shear (Figure 31) is likely to have occurred with annealing after the differential (shear) stress was removed. After the shear zone was abandoned and dropped down into a partly solidified LC granodiorite, the combination of latent heat from the pluton and lithostatic pressure from overlying sediments would yield flattening strains perpendicular to the shear zone boundaries. Vertical compression may account for the conjugate mica textures that mantle quartz and feldspar grains and help define foliation.

MYLONITE AND PROTOLITH GEOCHEMISTRY

Mylonite and granodiorite samples collected near the shear zone were analyzed for major and trace chemical composition to confirm a LC granodiorite protolith and to evaluate possible chemical changes from protolith to mylonite. This study determines that the LC granodiorite served as the mylonite protolith based on its location in the
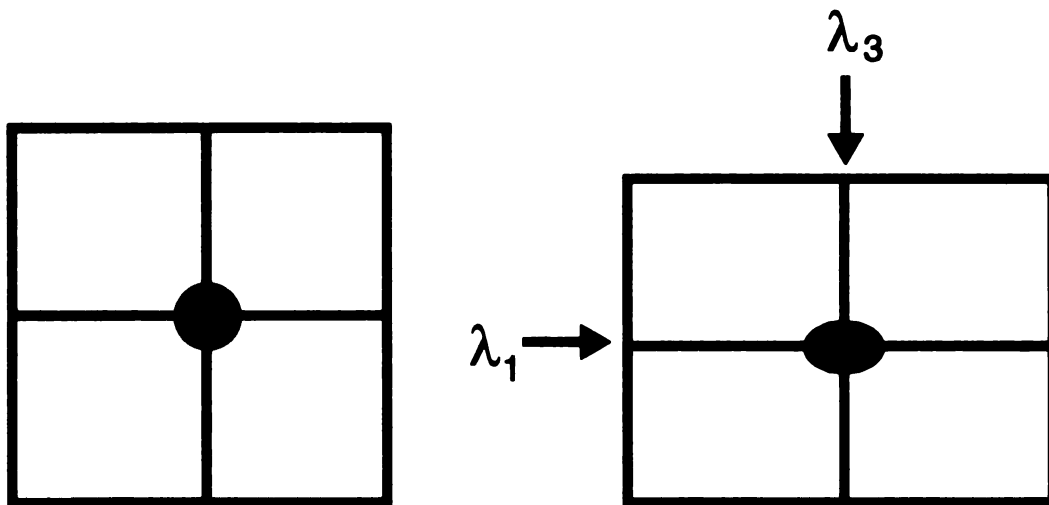
Figure 31. Simple illustration of flattening strains resulting from pure shear deformation. Note that the principal axes do not undergo rotation in pure shear. Post-shear flattening strains in the Silver Lake mylonite would result from lithostatic stresses acting on the shear zone after the removal of shear stress.

stock and

origin of

R

fluoresce

grain size

melted, u

a low-ter

oxidizer.

an orbital

S.MAX X

concentra

(Criss, 19

USGS sta

which the

standard t

Ei

chemical a

with Cr ar

all of whi

Appendix

alloy saw b

cracked du

stock and chemical similarity to the LC granodiorite. An alternative hypothesis for the origin of the shear zone is presented in the discussion.

Whole Rock Chemical Analyses

Representative samples of granodiorite and mylonite were analyzed by X-ray fluorescence (XRF) for major and trace elements. Using a volume appropriate for the grain size (e.g. fist-size for coarse-grained granodiorite), samples were powdered and melted, using 1.000 g of rock flour for each sample. Lithium Tetraborate was added as a low-temperature flux (9.000 g) and ammonium nitrate (0.160 g) was added as an oxidizer. Samples were melted in platinum crucibles (for > 25 min.) and stirred using an orbital mixing stage during heating. Fused disks were analyzed using a Rigaku S/MAX X-ray fluorescent spectrograph at Michigan State University. Major elements concentrations were determined using fundamental parameters to correct the analyses (Criss, 1980). Trace elements were done using accepted linear regression techniques on USGS standards. Table 4 in Appendix C lists major oxides and trace elements for which the samples were analyzed and detection limits in parts per million (ppm) for standard trace elements.

Eight mylonite samples and five granodiorite samples were selected for chemical analysis. One mylonite sample (8-97-17) appeared chemically contaminated with Cr and Ni abundances several orders of magnitude greater than any other sample, all of which had abundances of Cr and Ni below detection limits (see Table 4 in Appendix C). Elevated Cr and Ni abundances suggest possible contamination from an alloy saw blade during sectioning of billets (Vogel, pers. comm., 1998). One fused disk cracked during cooling (8-97-30) so a second disk was prepared for the sample and

analyzed a

Tables 5 a

samples.

Mylonite/

Se

mylonite a

mylonite a

protolith

samples, v

compared

Na₂O and

Th

These plo

abundance

compared

elemental

exception

between m

TiO₂, and 2

plot, accou

(n=5). Ra

enrichments

notable redu

analyzed along with the first disk. The two samples yielded very similar compostions. Tables 5 and 6 in Appendix C provide major and trace element compositions for the samples.

Mylonite/Protolith Comparison

Several major differences in chemical composition are apparent between mylonite and protolith samples. On a plot of SiO_2 vs. Al_2O_3 (Figure 32), samples of mylonite and granodiorite protolith are chemically distinct from one another. One protolith sample (8-97-30) shows consistently different composition from other samples, with low SiO_2. Overall, mylonite samples are markedly enriched in SiO_2 compared to the LC granodiorite. Conversely, mylonite samples show depletion in Na_2O and K_2O relative to granodiorites (Figure 33).

These variations and less obvious changes are seen in Figure 34 and Figure 35. These plots show mylonite/protolith ratios for all major and select trace element abundances, Rb and Zr. In Figure 34, a representative protolith sample (8-97-16) is compared to a representative mylonite (8-97-8) sample. Though varying in magnitude, elemental depletions and enrichments are consistent for all mylonite samples. The exception is a small range about one (0.965-1.095) for the ratio of Al_2O_3 abundance between mylonite and protolith. Mylonite samples are depleted in Na_2O, K_2O, CaO, TiO_2, and Zr, and enriched in MgO, SiO_2, MnO, FeO, and Rb. Figure 35 is a similar plot, accounting for larger protolith variations by averaging granodiorite abundances (n=5). Ratios are given for representative mylonite vs. average protolith. Here enrichments and depletions in the mylonite are consistent with Figure 34, except for a notable reduction in MgO and MnO enrichments and an overall depletion in FeO.

60
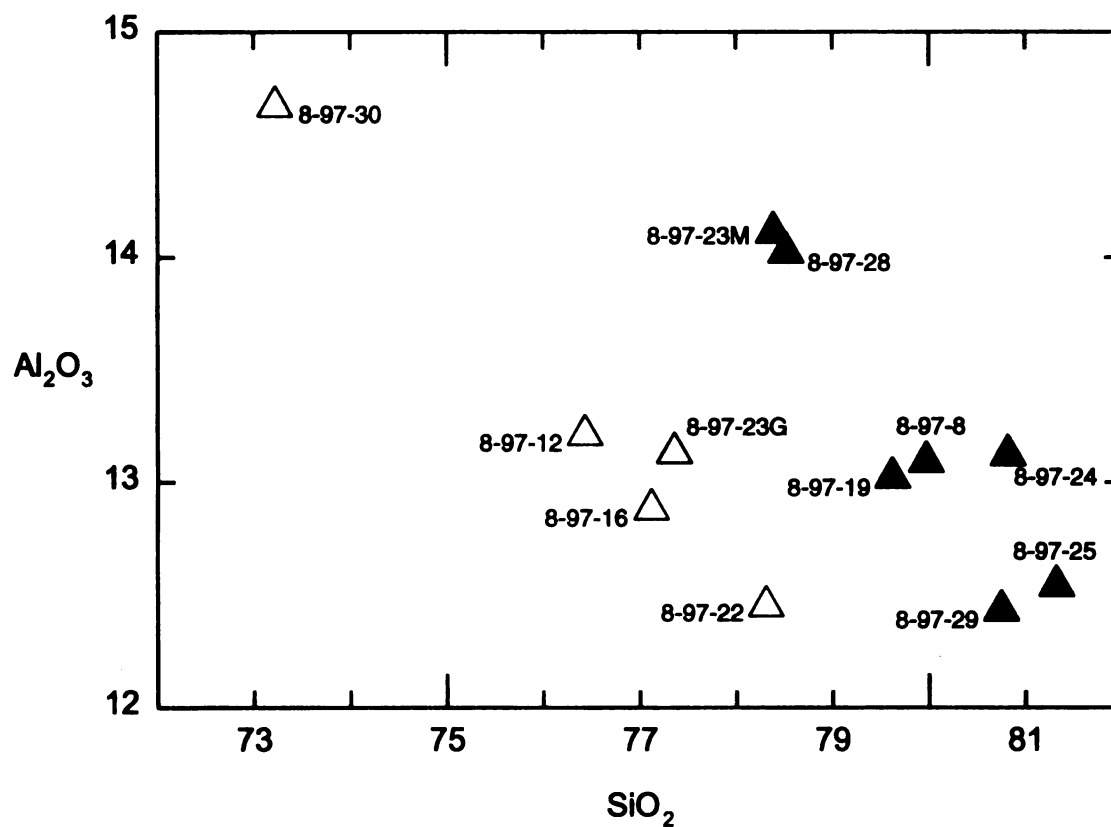
Al$_2$O$_3$

Figure

Figure 32. Plot of Al_2O_3 vs. SiO_2 for all granodiorite protolith and mylonite samples. Open triangles are granodiorite samples and closed triangles are mylonite samples. Note the general enrichment in SiO_2 of mylonite samples compared to those of the granodiorite protolith.

Na

K
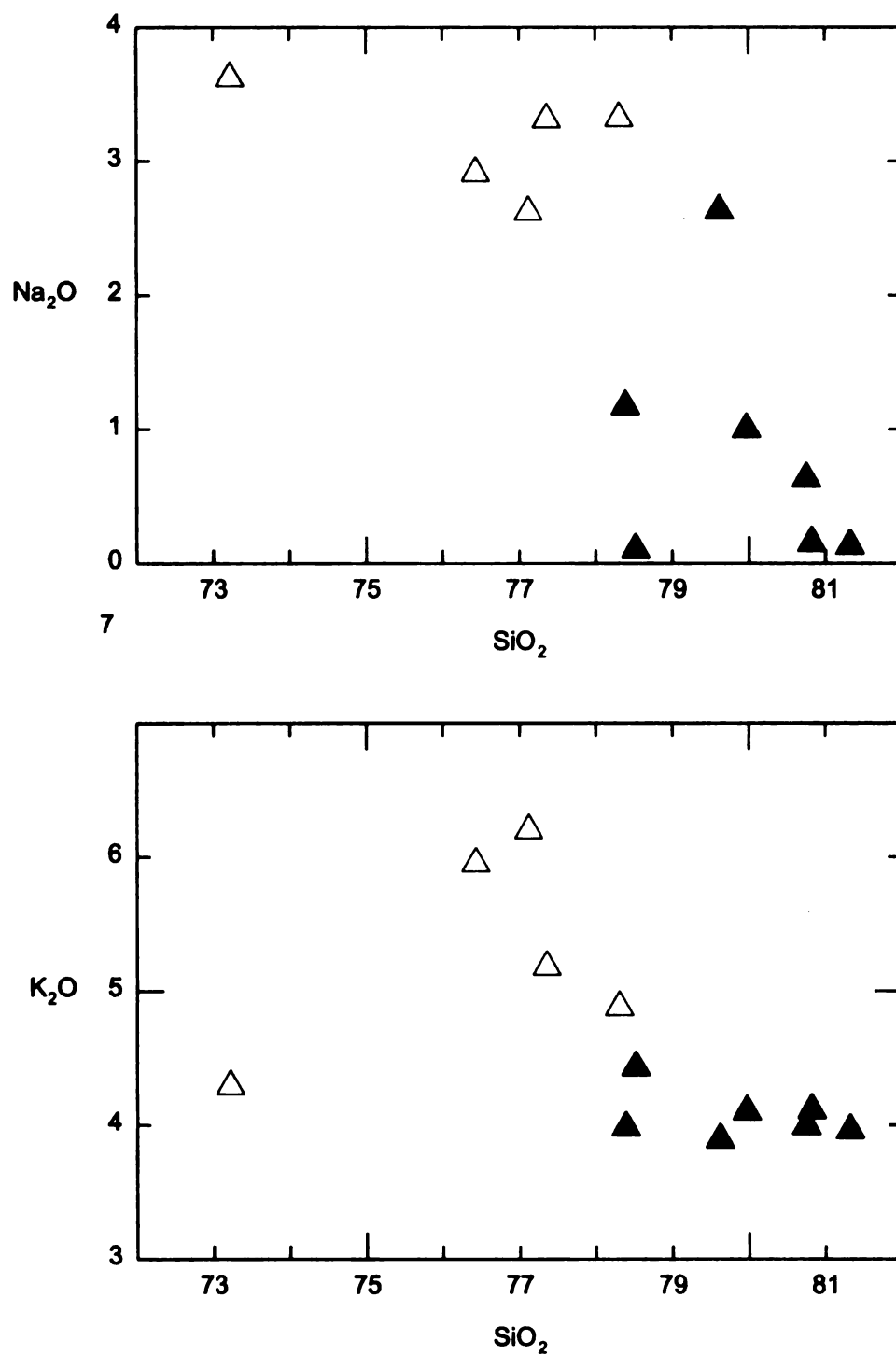
Figure 3

Figure 33. Plots of K_2O and Na_2O vs. SiO_2 for all granodiorite protolith and mylonite
samples. Open triangles are granodiorite samples and closed triangles are
mylonite samples. Note the general depletion of both K_2O and Na_2O in
mylonite samples compared to those of the granodiorite protolith.
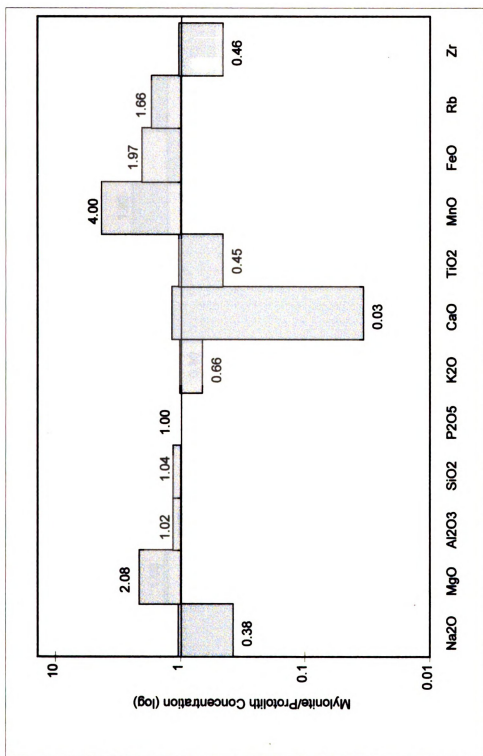
Figure 34. Major element and Rb, Zr concentration ratios for mylonite sample 8-97-8 versus granodiorite protolith 8-97-16.
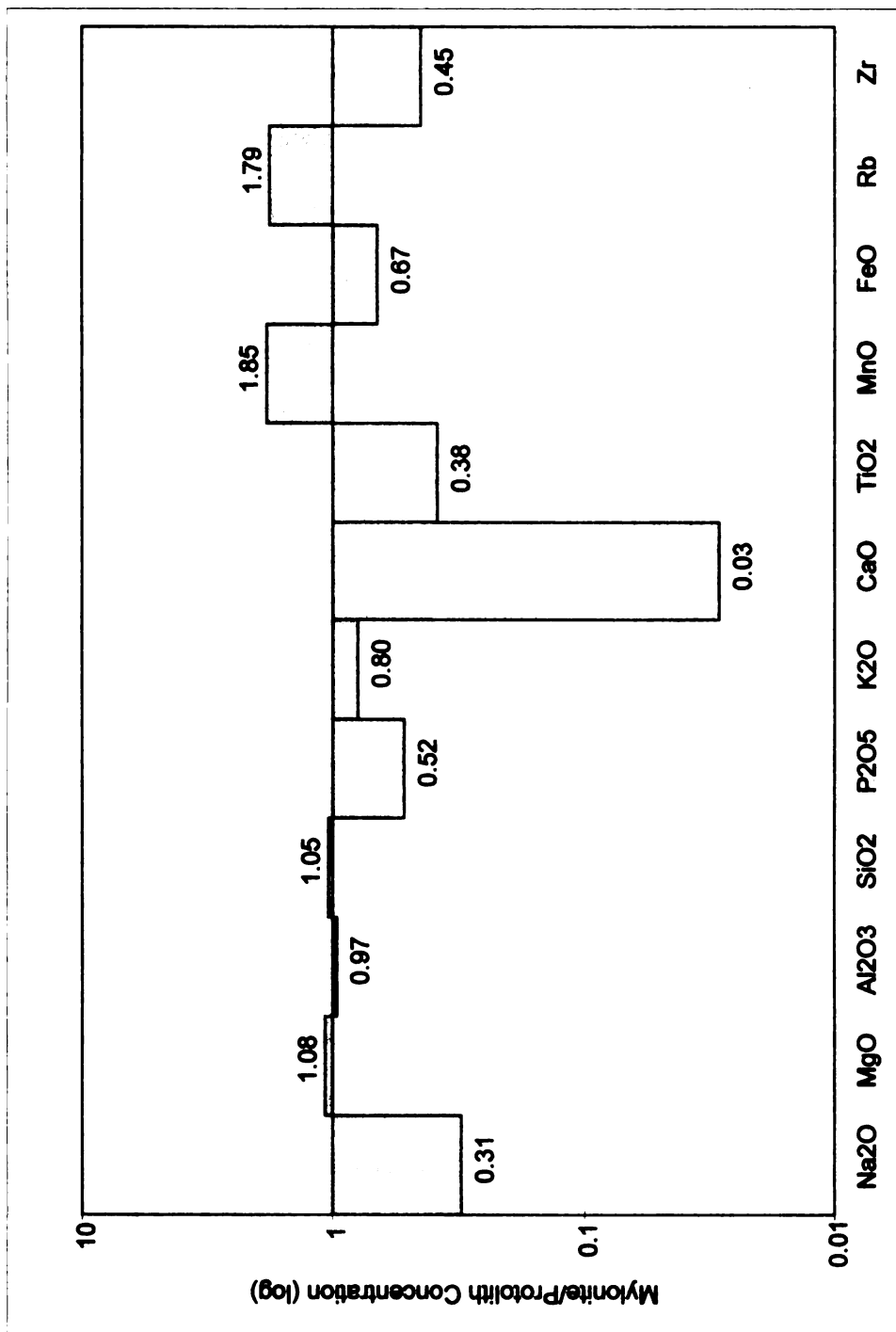
Figure 35. Major element and Rb, Zr concentration ratios for mylonite sample 8-97-8 versus average granodiorite protolith (n=5).

Alth

are conduits

Bell and C

mechanism

changes are

and out of t

unlikely to

xylonitizat

erther the t

assumed k

for the Si

concentrat

changes ca

elements (

St

fluid shea

O'Hara an

less consi

the eleme

often cite

to the flu

Discussion of Geochemical Data

Although many studies have shown that shear zones at low metamorphic grades are conduits for large volumes of hydrothermal fluids (Hippert, 1998; O'Hara, 1988), Bell and Cuff (1989) state that solution transfer is also a dominant deformation mechanism in phyllosilicate-bearing rocks at higher metamorphic grades. Chemical changes are often associated with mylonitization as mobile elements are transferred in and out of the shear zone in solution (Glazner and Bartley, 1991). As bulk chemistry is unlikely to balance during mass transfer, volume gains and losses may also accompany mylonitization. To characterize "metasomatic alterations," Gresens (1967) states that either the total volume change or the unique behavior of one species must be known or assumed known (i.e. which elements are immobile). There is no unique interpretation for the Silver Lake mylonite because neither volume change or individual element concentration changes are known. However, crude qualitative estimates of possible changes can be made based on the apparent behavior of commonly mobile or immobile elements (Glazner and Bartley, 1991; Gresens, 1967).

Studies have shown that Na, Si, K, and Rb are typically mobile in hydrothermal fluid shear zone systems, while Ti and Zr tend to be immobile (Bailey et al., 1994; O'Hara and Blackburn, 1989). The behavior of other elements (Mg, Al, Mn, Fe, Ca) is less consistent and similar studies have demonstrated both enrichment and depletion of the elements from protolith to mylonite. Enrichment of more immobile elements is often cited as evidence for volume loss in mylonites due to partitioning of Na, Si, and K to the fluid phase (O'Hara, 1990). Strain-softening reactions such as the breakdown of

ldspar into

solution (Hip

A v

ryionizati

based on ty

ample. de

mobile (Na

shown in Fi

and K ofte

enriched ir

producing

K_2O, CaO,

present in

W

lack of pro

quantfyir

of fluid co

volume c

behavior

a small

migrate

smaller

of this st

feldspar into micas have been suggested as one mode of freeing Si, K, Ca, and Na into solution (Hippert, 1998; O'Hara and Blackburn, 1989; O'Hara, 1988).

A volume change most likely accompanied chemical change during mylonitization in the Silver Lake shear zone. The concentration changes are perplexing based on typically mobile and immobile elements in hydrothermal systems. For example, depletion of commonly immobile elements (Ti, Zr) is unexpected if typically mobile (Na, K) elements have been transferred out of the shear zone in solution. As shown in Figure 34, Ti, Zr, Na, and K are all depleted in the mylonite. In addition, Rb and K often behave similarly in hydrothermal systems. Mylonites are comparatively enriched in Rb, but relatively depleted in K_2O, CaO, and Na_2O (Figure 35). Mica-producing reactions involving feldspar breakdown may be responsible for freeing SiO_2, K_2O, CaO, and Na_2O. This reaction is consistent with the abundance of white micas present in mylonite samples, but does not explain the Rb enrichment.

Without knowledge of an absolute loss or gain in any element, coupled with the lack of predictable behavior of any species, there are an infinite number of solutions to quantifying volume changes and mass transfer in the Silver Lake shear zone. A number of fluid compositions with varying saturation states could be responsible for a range of volume changes. A second postulate is given by Hippert (1998) who also noted erratic behavior in mobile and immobile elements from protolith to mylonite accompanied by a small volume gain inferred from concentration changes. Individual elements may migrate heterogeneously through and within a shear zone system, accounting for smaller than outcrop-scale volume changes (Hippert, 1998) not considered in the scale of this study.

DISCU

Signif

Stock

the L

strong

shear

the p

Figur

LC g

the I

folds

The

(Fig

myl

min

gran

(Co

the

inte

the

DISCUSSION AND CONCLUSIONS

Significance of the Silver Lake Mylonite: Structural Setting and Chemistry

Before evaluating structural models of emplacement for the Little Cottonwood Stock, it is important to restate the relationship between the Silver Lake mylonite and the LC granodorite, including the nature of the protolith. Several lines of evidence strongly support the following conclusions. 1.) The Silver Lake mylonite is part of a shear zone that formed at or near the pluton/wallrock contact during emplacement of the pluton. 2.) The mylonite was down-dropped at the base of the Mdo block shown in Figure 17 and the shear zone was abandoned in favor of a new detachment surface. 3.) LC granodiorite was the protolith for the mylonite.

The location and orientation of the shear zone suggest that shearing occurred at the LC/Mdo contact. Although shear sense in the mylonite remains unclear, sheath folds and lineations support shear in a plane dipping moderately to the west-southwest. The orientation of the shear zone is similar to that of the LC/Mdo contact in the area (Figure 5). Timing is well constrained by radiometric dating of shear zone and mylonite samples. $^{40}Ar/^{39}Ar$ whole-rock data from mylonite samples provides a minimum slip age on the shear zone of ~27 Ma. U/Pb and $^{40}Ar/^{39}Ar$ dating for granodiorites on either side of the shear zone yield closure ages of ~ 30 Ma (Constenius, 1998; Vogel et al., 1997; Layer and Damon, pers. comm., 1998). Slip on the shear zone after closure of the granodiorite (i.e. pre-full crystallization) supports the interpretation that shearing occurred during final crystallization, or emplacement, while the magma was in a semi-solid state.

67

Th

granodiori

The lack

typothesi

middle Ca

sandstone

lithology

dike trun

possibilit

intruded

Evaluati

T

determin

Based o

direction

producir

Lake de

m) were

west wa

7

in a rele

(1998) a

model.

The bulk chemical composition of the mylonite is similar to that of the granodiorite. None of the samples, mylonite or granodiorite, have >1.72 wt. % CaO. The lack of significant CaO precludes a calcareous Mdo protolith. An alternative hypothesis is that the mylonite is a piece of sheared quartzite from one of the lower to middle Cambrian units that underlie the Mdo, either Tintic Quartzite (ϵt) or a shaly sandstone member of the Ophir Formation (ϵo). However, given the adjacent Mdo lithology and pattern of faulting, this scenario is unlikely. In addition, the age of the dike truncated by the mylonite (27.0 $\pm$ 0.3 Ma, whole rock $^{40}Ar/^{39}Ar$) excludes the possibility that the mylonite is derived from sheared roof rock sediments, since the dike intruded before shearing (27.1 $\pm$ 0.1 Ma).

Evaluation of Emplacement Models

The purpose of this study was to describe the Silver Lake mylonite in detail and determine its relevance to an emplacement mechanism for the Little Cottonwood stock. Based on the preceding evidence, syn-emplacement shearing occurred in an east-west direction at the roof contact between the Little Cottonwood Stock and Mdo wallrocks, producing the Silver Lake mylonite. The shear zone was originally part of the Silver Lake detachment fault of Constenius (1998). The mylonite and overlying Mdo (~100 m) were then dropped down by a normal fault, producing the half-graben seen on the west wall of Silver Lake cirque.

The data presented in this study could be interpreted as support for emplacement in a releasing step along a west-dipping normal fault in the models of both Constenius (1998) and Vogel et al. (1997), although the extension direction is different in each model. In the Vogel et al. (1997) model, emplacement occurs within a releasing step

associated with a releasing bend along an east-west trending strike slip fault. This model is not rejected by evidence in the Silver Lake mylonite. The overall orientation of the dikes supports this model, where left-lateral movement along the strike slip fault was responsible for regional extension in a northwest-southeast direction. East-west shearing at the roof of the pluton allows for westward movement of the Silver Lake detachment hanging wall during local extension on a releasing step within the releasing bend (Figure 16). In this model, local extension within the releasing bend is east-west and overall regional extension is northwest-southeast.

In the model presented by Constenius (1998), the transport direction for the C-N thrust sheet is west (or southwest). Constenius (1998) states that the distribution of sheath fold hinge lines and several lineation measurements in the Silver Lake mylonite "suggest an east-west, perhaps a more southerly extension direction" for the Silver Lake detachment. The east-west shear direction obtained from sheath folds in this study would also support an interpretation that the Silver Lake detachment is part of the overall network of faults that accommodated regional east-west extension during westward collapse of the cordillera.

Neither the model of Constenius (1998) or Vogel et al. (1997) is rejected by evidence for shear direction in the Silver Lake mylonite, yet the models are not in agreement with regard to regional extension. Left-lateral displacement along an east-west trending strike slip fault in the Vogel et al. (1997) model is consistent with the orientation of dike swarms. However, motion on the same fault during west or southwest transport of the C-N allochthon would be right-lateral. In the following model for emplacement of the Little Cottonwood Stock, it is suggested that westward

collapse of the cordillera and emplacement of the stocks and dikes are associated with separate tectonic events and do not represent contradictory interpretations of the evidence.

Composite Model: An Emplacement Mechanism for the Little Cottonwood Stock

Many studies have proposed that plutons are often emplaced as tabular bodies, which contrasts the popularized notion of balloon-shaped diapirs that force their way into the crust. Plutons are commonly tabular and their shape may be invariant of pluton size (McCaffrey and Petford, 1997). Cruden (1998) recently suggested that the widespread occurrence of tabular plutons is the result of an efficient emplacement process that simply exchanges material within the crust. As magma is withdrawn from its source region, it ascends vertically through dikes or dike networks until it reaches a mechanical barrier that prevents further ascent (e.g. free surface, neutral buoyancy). Many workers (e.g. Clemens and Mawer, 1992) suggest that vertical fracture propagation and dike transport is an efficient ascent mechanism for granitoid magmas. As the magma spreads laterally at the mechanical barrier, the pluton floor is depressed toward the depleted region of generation. The system acts essentially as either a piston or a cantilever (Figure 36). Cruden (1998) notes that both the flow rates through dikes and strain rates in the crust are geologically reasonable for this process, and the mechanism can operate synchronously with tectonic emplacement mechanisms.

This study suggests that mutiple near-field and far-field MTPs operated around the Little Cottonwood Stock during emplacement. Emplacement was a result of dike-fed filling of a tectonically created cavity along a releasing step on a dip slip fault within a releasing bend. (The composite fault model is described on page 29.) Upon

70
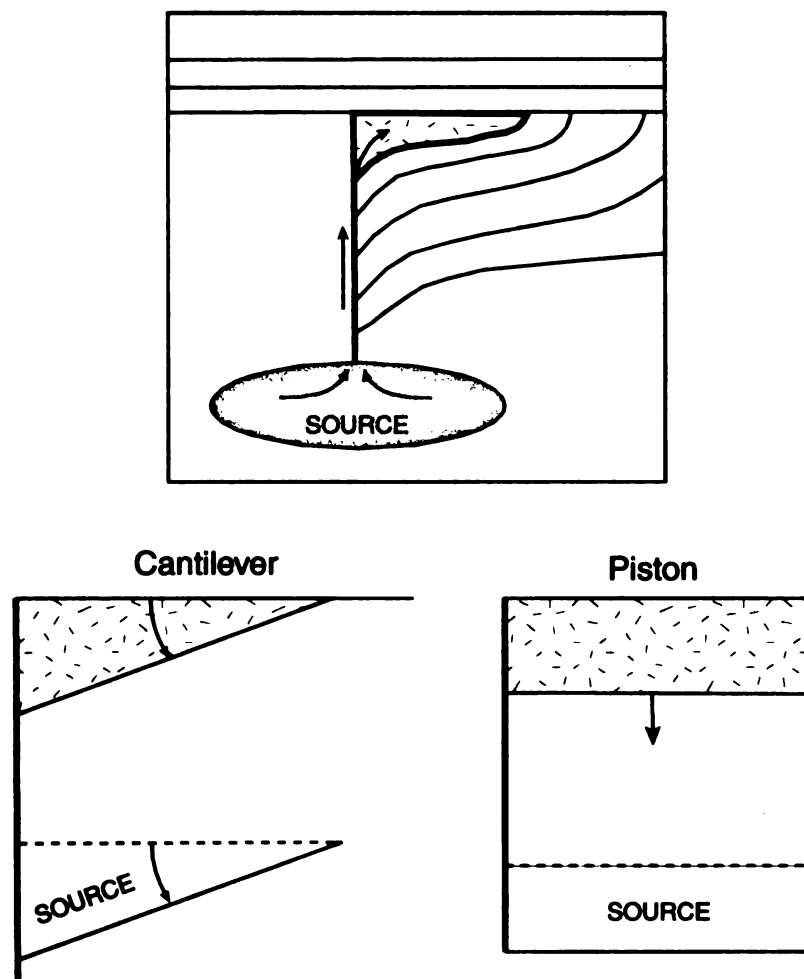
Figure 36. Schematic diagrams showing the material exchange process in the
floor subsidence model of Cruden (1998). The upper diagram shows
a magma chamber emplaced by means of lowering crustal material
into a deflating source region. Material is transported by the dike on
the left-hand side of the diagram. The two lower diagrams show the
subsidence mechanisms for downward displacement of the crustal
material, the cantilever and piston models. All diagrams modified
from Cruden (1998).

71

reaching a mechanical barrier to further ascent, the magma intruded wallrocks laterally. A small amount material transfer may have occurred by other emplacement mechanisms, such as stoping (Paterson et al., 1996; Paterson et al., 1991).

Figure 37 illustrates the proposed emplacement model for the Little Cottonwood Stock. The Archean-Proterozoic suture provided a structural weakness in the crust for the ascent of magmas generated in or at the base of the lower crust (Feher, 1997; Presenell, 1997). Magmas ascended to mid-crustal levels during a period of deep-seated northwest-southeast extension. A tectonic cavity opened along a releasing step on a west-dipping dip slip fault associated with a releasing bend along an east-west trending strike slip fault. Although evidence for the fault has not been found, the location of the strike slip fault proposed in this study is shown on the inset map in Figure 37.

Cenozoic collapse of the Cordilleran wedge beginning in the Paleogene may have been contemporaneous with slip on the east-west strike slip fault responsible for producing the tectonic cavity. However, in this model the local east-west extension in the releasing bend is uncoupled from west-southwest transport (i.e. extension) of the C-N allochthon, which is bound by the Deer Creek Fault to the north. Although the events may be temporally related, they need not be products of the same tectonic regime. Westward collapse of the cordillera (i.e. the C-N thrust sheet) occurred faster than deep-seated strain in the crust, which would result in an overall right-lateral sense of shear on portion of the strike slip fault south of the Little Cottonwood Stock.

Concomitant with the opening, the magma reached a mechanical barrier to further ascent, most likely the slip surface on the detachment of the releasing step
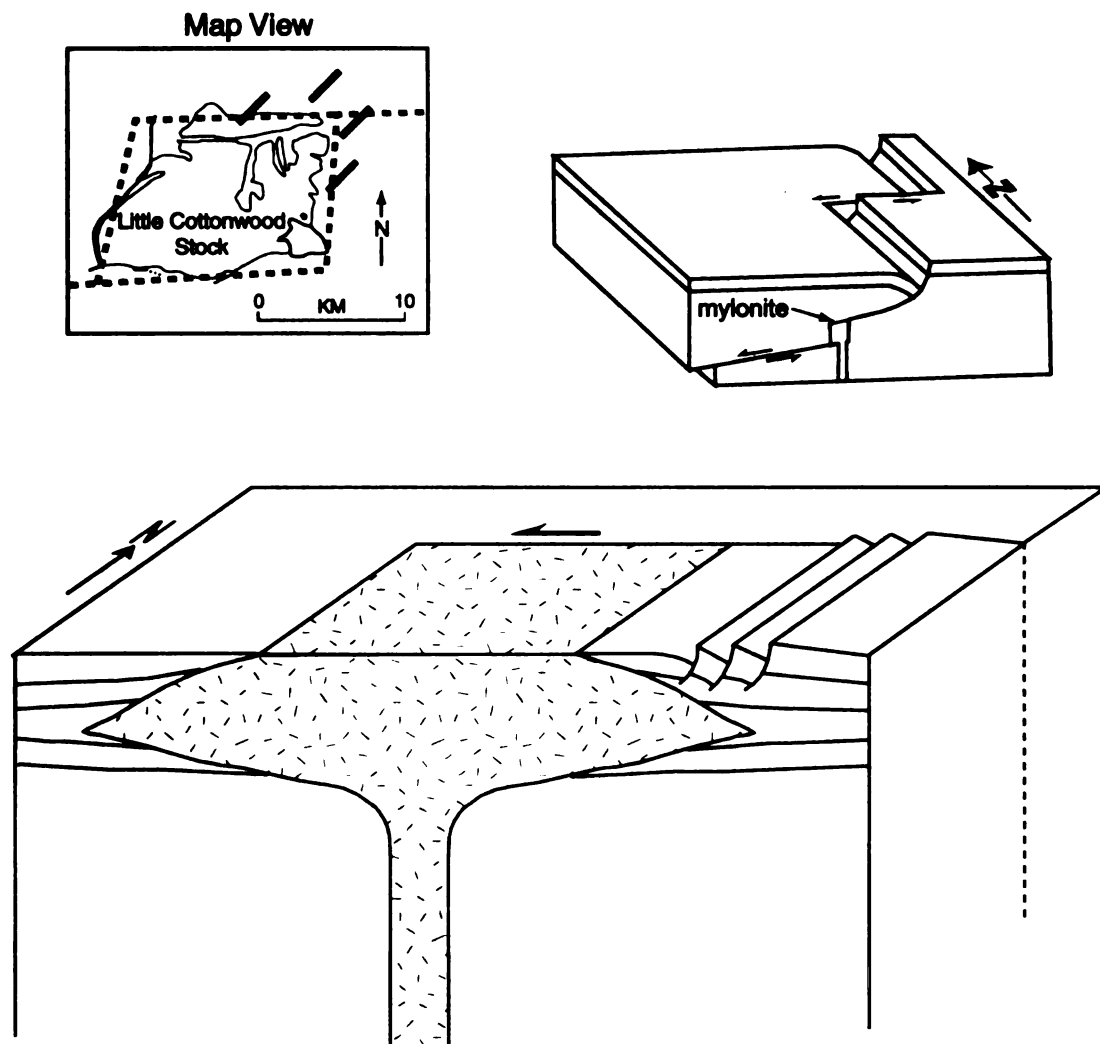
Figure 37. Emplacement model for the Little Cottonwood Stock. The inset map shows the approximate trend of the east-west strike slip fault in the model. The illustration in the upper right corner shows initial intrusion of the stock into the releasing step. The magma ascends into the step through the feeder dike. As the magma reaches the detachment surface it stops rising and fills the chamber concomitant with tectonic opening. Late-stage emplacement is illustrated in the lower diagram, where continued intrusion has effectively obliterated evidence of the releasing step. The component of forcible intrusion is shown along bedding.

(Figure 37). Shearing occurred at the roof during emplacement, producing the Silver Lake mylonite. With progressive slip along the dip slip fault, the intrusion effectively obliterated the step, illustrated by the transition between the two diagrams in Figure 37. A series of normal faults dropped the mylonite down at the base of a half-graben, and repeatedly cut sequences of beds east of the pluton. During episodic pulses of magma, when the rate of influx exceeded the rate of tectonic opening, the magma intruded wallrocks on the western and eastern sides of the pluton concordantly.

APPENDIX A

FIELD METHODS

Field work was conducted in two phases during the summer field seasons of 1997 and 1998. The first phase lasted two weeks during August, 1997 and included examining and sampling exposed contacts on the northern, eastern and southern margins of the pluton (see Figure 3). Contacts were examined for macro- and mesoscopic evidence of deformation resulting from emplacement, including the presence of kinematic or sense-of-shear indicators. Twenty-nine oriented samples were collected from the contacts, taken in regular intervals toward the interior of the pluton, based on observed textures. At a typical locale, samples were taken in 1, 5, and 10 m spacings from the contact. The majority of the first phase was dedicated to detailed measurement and description of the shear zone located near the southeast exposure of the stock. Sheath folds and mineral lineations on fold limbs were measured across the exposed shear zone (17 m x 0.5 m in cross-section) and selectively sampled, usually in less than 2.0 m spacings based on the high aspect ratio of the tabular zone. Fifteen mylonite samples and eight granodiorite samples from near the shear zone were collected. Fold axes, hinge lines, and mineral lineations were measured directly on the outcrop when possible. In many cases, thin wooden skewers and adhesive were used to extend hinge lines from the plane of the outcrop.

The second phase of field work was conducted for one week in September, 1998, during which the shear zone and adjacent LC and Mdo rocks were mapped at a scale of 1:2400 (Figure 5). Using traditional baseline mapping techniques, the map was produced for an area of approximately 33,400 m^2. Wallrock medasediments at the contact were also examined for the presence of intrusion- and fault-related deformation.

APPENDIX B

Table 1. Field measurements collected for mafic enclaves in the Silver Lake area and corresponding ϕ' and R_f values.

Trend of Long Axis (degrees)	ϕ'	Long Axis (cm)	Short Axis (cm)	R_f
166	-14	12.1	5.8	2.09
154	-26	8.4	4.5	1.87
144	-36	7.2	3.5	2.06
229	49	12.4	8.7	1.43
94	-86	12.6	8.3	1.52
228	48	6.1	3.7	1.65
230	50	9.7	5.2	1.87
181	1	9.8	4.3	2.28
191	11	13.4	5.1	2.63
167	-13	10.2	4.9	2.08
200	20	8	4.4	1.82
171	-9	11.8	4.6	2.57
146	-34	7.1	2.9	2.45
170	-10	11.7	5.8	2.02
122	-58	8.1	5.2	1.56
226	46	32.8	24.2	1.36
161	-19	12.1	6.1	1.98
114	-66	8.2	4.2	1.95
208	28	6.3	2.0	3.15
245	65	5.2	2.1	2.48
189	9	7	3.8	1.84
186	6	14.2	6.0	2.37
152	-28	10.8	4.9	2.20
208	28	4.5	3.0	1.50
204	24	4	2.6	1.54
186	6	4.9	3.9	1.26
204	24	9.4	7.8	1.21
235	55	16	12.1	1.32
161	-19	7.3	4.4	1.66

Table 2. Measurements for axial surfaces and hinge lines on sheath folds and lineations on foliation surfaces in the Silver Lake mylonite. All measurements reported in azimuth.

Domain	Fold	Axial Surface	Hinge Line	Lineation	Foliation
A	1	297/34	002/09	281/30	254/34
			227/19	279/00	321/21
				246/27	295/42
B	1	241/28	271/35	299/27	260/34
				266/24	
	2	250/42	253/47	296/31	
				266/42	
				291/29	
				289/25	
C	1	301/16	178/12	333/39	284/27
				335/35	
	2		238/20	320/21	
			211/25	325/17	315/20
				313/20	
	3	284/30	353/11	145/50	132/60
				335/40	284/27
				287/22	
				260/17	
				332/24	295/27
				328/14	319/14
				280/11	295/27
				253/45	281/53
				223/35	
				205/25	
D	1	256/21	206/14	261/02	231/09
				281/09	316/21
	2	222/09	196/21		
	3	291/18	011/11		
E	1	245/13	180/28	152/14	
			166/18	259/01	195/24
			154/26	217/19	
			196/25	202/19	
				206/20	
	2		209/31		
			199/37		
			104/20		

Table 2. (cont'd).

Domain	Fold	Axial Surface	Hinge Line	Lineation	Foliation
F	1	249/20	349/03	344/01	084/04
			310/13	301/15	010/36
			292/16	296/26	239/49
G	1	261/32	320/20	324/16	009/16
			324/19	318/28	335/27
			324/15	298/18	246/18
	2	248/21	301/15		

APPENDIX C

Table 3.   CIPW norm calculations for two mylonite samples and averaged protolith (n=5). Note the increased abundance of quartz in mylonites compared to the average protolith and the predicted dominance of quartz and feldsapr in mylonite samples. M = mylonite. Values were calculated using Igpet for Windows (Carr, 1994).

	Ave. Protolith	8-97-8 (M)	8-97-25 (M)
	n = 5	n = 1	n =1
%Anorthite	15.23	0.21	9.64
Quartz	34.25	57.59	63.4
Orthoclase	30.34	24.23	23.4
Albite	27.42	8.46	1.1
Anorthite	4.93	0.02	0.12
Corundum	0.81	7	8
Hypersthene	2.02	1.7	4.06
Ilmenite	0.25	0.09	0.09
Apatite	0.09	0.05	0.05
TOTAL	100.09	99.14	100.22

Table 4. Detection limits for trace elements by XRF analysis of glass disks and statistical variance of major oxide analyses based on a USGS standard treated as an unkown.

Element	Detection Limit (ppm)
Ba	100
La	48
Cr	63
Ni	25
Zn	14
Rb	13
Sr	12
Y	14
Nb	15
Zr	14

Major Oxide	Standard Deviation
SiO_2	0.106
TiO_2	0.009
$Al2O_3$	0.077
FeO	0.030
MnO	0.004
MgO	0.018
CaO	0.014
Na_2O	0.018
K_2O	0.002
P_2O5	0.005

Table 5. XRF whole rock chemical data for major oxides. (G = granodiorite protolith, M = mylonite.)

Sample #	SiO_2	Al_2O_3	FeO	MgO	CaO	Na_2O	K_2O	TiO_2	P_2O_5	MnO
8-97-12 (G)	76.43	13.21	0.9	0.2	0.71	2.91	5.95	0.11	0.03	0.02
8-97-16 (G)	77.12	12.88	0.3	0.12	0.89	2.62	6.2	0.11	0.02	0.01
8-97-22 (G)	78.31	12.45	1.02	0.13	0.5	3.32	4.88	0.09	0.03	0.02
8-97-23 (G)	77.36	13.13	0.74	0.1	0.73	3.31	5.18	0.09	0.02	0.02
8-97-30 (G)	72.82	14.64	1.32	0.4	1.71	3.66	4.3	0.19	0.06	0.03
8-97-30 (G)	73.22	14.67	1.01	0.44	1.72	3.62	4.29	0.19	0.07	0.03
8-97-8 (M)	79.97	13.09	0.59	0.25	0.03	1	4.1	0.05	0.02	0.04
8-97-17 (M)	73.14	12.84	1.2	0.34	2.3	2.32	3.11	0.06	0.02	0.1
8-97-19 (M)	79.62	13.02	0.7	0.21	0.1	2.63	3.89	0.05	0.02	0.05
8-97-23 (M)	78.39	14.11	0.89	0.36	0.05	1.17	3.98	0.06	0.02	0.03
8-97-24 (M)	80.82	13.12	0.49	0.29	0.03	0.15	4.11	0.05	0.02	0.03
8-97-25 (M)	81.32	12.54	1.8	0.3	0.05	0.13	3.96	0.05	0.02	0.05
8-97-28 (M)	78.52	14.02	0.61	0.3	0.17	0.1	4.43	0.06	0.02	0.05
8-97-29 (M)	80.75	12.43	0.67	0.28	0.05	0.63	3.99	0.05	0.02	0.04

Table 6. XRF whole rock chemical data for trace elements. (G = granodiorite protolith, M = mylonite, *ND* = not detected.)

Sample #	Cr	Ni	Cu	Zn	Rb	Sr	Y	Zr	Nb	La	Ba
8-97-12 (G)	*ND*	*ND*	*ND*	*ND*	130	148	*ND*	56	*ND*	*ND*	378
8-97-16 (G)	*ND*	*ND*	*ND*	*ND*	180	203	*ND*	69	*ND*	*ND*	370
8-97-22 (G)	*ND*	*ND*	*ND*	*ND*	186	43	*ND*	67	20	*ND*	53
8-97-23 (G)	*ND*	*ND*	*ND*	*ND*	177	201	*ND*	49	*ND*	*ND*	849
8-97-30 (G)	*ND*	*ND*	*ND*	20	162	407	15	104	*ND*	*ND*	1341
8-97-30 (G)	*ND*	*ND*	*ND*	18	162	406	*ND*	82	*ND*	*ND*	1272
8-97-8 (M)	*ND*	*ND*	*ND*	43	297	*ND*	18	32	46	*ND*	131
8-97-17 (M)	*ND*	124	*ND*	36	292	160	18	43	43	*ND*	*ND*
8-97-19 (M)	*ND*	*ND*	*ND*	29	236	25	14	33	38	*ND*	248
8-97-23 (M)	*ND*	*ND*	*ND*	52	323	*ND*	*ND*	43	42	*ND*	*ND*
8-97-24 (M)	*ND*	*ND*	*ND*	45	299	*ND*	19	42	41	*ND*	*ND*
8-97-25 (M)	*ND*	*ND*	*ND*	56	327	*ND*	22	45	39	*ND*	*ND*
8-97-28 (M)	*ND*	*ND*	*ND*	60	355	*ND*	35	47	47	*ND*	165
8-97-29 (M)	*ND*	*ND*	*ND*	59	317	*ND*	32	42	37	*ND*	132

REFERENCES CITED

REFERENCES CITED

Bailey, C.M., Simpson, C., and De Paor, D.G., 1994,Volume loss and tectonic flattening strain in granitic mylonites from the Blue Ridge province, central Appalachians, Journal of Structural Geology, v. 16, p. 1403-1416.

Bell, T.H., and Cuff, C., 1989, Dissolution, solution transfer, diffusion versus fluid flow and volume loss during deformation/metamorphism, Journal of Metamorphic Geology, v. 7, p. 425-447.

Bromfield, C.S., Erickson, A.J., Haddadin, M.A., and Mehnert, H.H., 1977, Potassium-argon ages of intrusion, extrusion, and associated ore deposits, Park City Mining District, Utah, Economic Geology, v. 72, p. 837-848.

Brown, M., 1994, The generation, segregation, ascent and emplacement of granite magma: the migmatite-to-crustally-derived granite connection in thickened origins, Earth-Science Reviews, v. 36, p. 83-130.

Cambray, F.W., Vogel, T.A., and Mills, J.G., 1995, Origin of compositional heterogeneities in tuffs of the Timber Mountain Group: The relationship between magma batches and magma transfer and emplacement in an extensional environment, Journal of Geophysical Research, v. 100, p. 15793-15805.

Carr, M.J., 1994, Igpet for Windows, Terra Softa Inc., Somerset, N.J., USA.

Christiansen, P.P., and Pollard, D.D., 1997, Nucleation, growth and structural development of mylonitic shear zones in granitic rock, Journal of Structural Geology, v. 19, p. 1159-1172.

Clemens, J.D., 1998, Observations on the origins and ascent mechanisms of granitic magmas, Journal of the Geological Society, London, v. 155, p. 843-851.

Clemens, J.D., and Mawer, C.K., 1992, Granitic magma transport by fracture propagation, Tectonophysics, v. 204, p. 339-360.

Cobbold, P.R., and Gapais, D., 1987, Shear criteria in rocks: an introductory review, Journal of Structural Geology, v. 9, p. 521-523.

Cobbold, P.R., and Quinquis, H., 1980, Development of sheath folds in shear regimes, Journal of Structural Geology, v. 2, p. 119-126.

Coney, P.J., and Harms, T.A., 1984, Cordilleran metamorphic core complexes: Cenozoic extensional relics of Mesozoic compression, Geology, v. 12, p. 550-554.

Constenius, K.N., 1998, Extensional tectonics of the Cordilleran foreland fold and thrust belt and the Jurassic-Cretaceous Great Valley forearc basin, Ph.D Dissertation, The University of Arizona, 116 pp.

Constenius, K.N., 1996, Late Paleogene extensional collapse of the Cordilleran foreland fold and thrust belt, GSA Bulletin, v. 108, p. 20-39.

Covey-Crump, S.J., 1997, The high temperature static recovery and recrystallization behavior of cold-worked Carrara marble, Journal of Structural Geology, v. 19, p. 225-241.

Crispini, L., and Capponi, G., 1997, Quartz fabric and strain partitioning in sheath folds: an example from the Voltri Group (Western Alps, Italy), Journal of Structural Geology, v. 19, p. 1149-1157.

Criss, J., 1980, Fundamental parameter calculations on a laboratory microcomputer, Advances in X-ray Analysis, v. 23, 93-97.

Crittenden, M.D., Stuckless, J.S., Kistler, R.W., and Stern, T.W., 1973, Radiometric dating of intrusive rocks in the Cottonwood Area, Utah, U.S. Geological Survey Journal of Research, v. 1, p. 173-178.

Crittenden, M.D., Jr., 1965, Geology of the Dromedary Peak Quadrangle, Utah: U.S. Geological Survey Geologic Quadrangle Map GQ-378.

Cruden, A.R., 1998, On the emplacement of tabular granites, Journal of the Geological Society, London, v. 155, p. 853-862.

Cruden, A.R., 1990, Flow and fabric development during the diapiric rise of magma, Journal of Geology, v. 98, p. 681-698.

Cruden, A.R., 1988, Deformation around a rising diapir modeled by creeping flow past a sphere, Tectonics, v. 5, p. 1091-1101.

England, R.W., 1990, The identification of granitic diapirs, Journal of the Geological Society, London, v. 147, p. 931-933.

Feher, L.A., 1997, Petrogenesis of the Keetley Volcanics, in Summit and Wasatch Counties, North-central Utah, M.S. Thesis, Michigan State University, 95 pp.

Feher, L.A., Constenius, K.N., and Vogel, T.A., 1996, Relationships between the Wasatch Intrusive Belt and Keetley Volcanics, north-central Utah, Geological Society of America Annual Meeting, Abstracts with Programs, v. 28, no. 7.

Fowler, T.K., and Paterson, S.R., 1997, Timing and nature of magmatic fabrics from structural relations around stoped blocks, Journal of Structural Geology, v. 19, p. 209-224.

Glazner, A.F., and Bartley, J.M., 1991, Volume loss, fluid flow and state of strain in extensional mylonites from the central Mojave Desert, California, Journal of Structural Geology, v. 13, p. 587-594.

Gresens, R.L., 1967, Composition-volume relationships of metasomatism, Chemical Geology, v. 2, p. 47-65.

Hippertt, J.F., 1998, Breakdown of feldspar, volume gain and lateral mass transfer during mylonitization of granitoid in a low metamorphic grade shear zone, Journal of Structural Geology, v. 20, p. 175-193.

Hobbs, B.E., Means, W.D., and Williams, P.F., 1976, *An Outline of Structural Geology*, John Wiley and Sons, 571 pp.

Hudleston, P.J., 1986, Extracting information from folds in rocks, Journal of Geological
Education, v. 34, p. 237-245.

Hutton, D.H.W., 1997, Syntectonic granites and the principle of effective stress: A
general solution to the space problem? *in* Granite: From segregation of melt to
emplacement fabrics, Bouchez, J.L., Hutton, D.H.W., and Stephens, W.E., eds.,
Kluwer Academic Publishers, p. 189-197.

Hutton, D.H.W., 1988, Granite emplacement mechanisms and tectonic controls:
inferences from deformation studies, Transactions of the Royal Society of
Edinburgh: Earth Sciences, v. 79, p. 245-255.

John, D.A., 1997, Geologic setting and characteristics of mineral deposits in the central
Wasatch Mountains, Utah *in* John, D.A., and Ballantyne, G.H., eds., Geology
and Ore Deposits of the Oquirrh and Wasatch Mountains, Utah, Society of
Economic Geologists Guidebook Series, v. 29, p. 15-45.

John, D.A., 1989, Geologic setting, depths of emplacement, and regional distribution of
fluid inclusions in intrusions of the central Wasatch Mountains, Utah, Economic
Geology, v. 84, p. 386-409.

John, D.A., Turrin, B.D., and Miller, R.J., 1997, New K-Ar and 40Ar/39Ar ages of
plutonism, hydrothermal alteration, and mineralization in the central Wasatch
Mountains, Utah *in* John, D.A., and Ballantyne, G.H., eds., Geology and Ore
Deposits of the Oquirrh and Wasatch Mountains, Utah, Society of Economic
Geologists Guidebook Series, v. 29, p. 65-79.

Karlstrom, K.E., Miller, C.F., Kingsbury, J.A., and Wooden, J.L., 1993, Pluton
emplacement along an active ductile thrust zone, Piute Mountains, southeastern
California: Interaction between deformational and solidification processes,
Geological Society of America Bulletin, v. 105, p. 213-230.

Lawton, T.F., 1980, Petrography and structure of the Little Cottonwood Stock and
metamorphic aureole, Central Wasatch Mountains, Utah, M.S. Thesis, Stanford
University, 76 pp.

Marsh, B.D., 1982, On the mechanics of igneous diapirism, stoping, and melting,
American Journal of Science, v. 282, p. 808-855.

90

McCa

O'Har

O'Har

O'Har

Paters

Pater

Pater

Pate

Pres

Rar

McCaffrey, K.J.W., and Petford, N., 1997, Are granitic intrusions scale invarient?, Journal of the Geological Society, London, v. 154, p. 1-4.

O'Hara, K., 1990, State of strain in mylonites from the western Blue Ridge province, southern Appalachians: the role of volume loss, Journal of Structural Geology, v. 12, p. 419-430.

O'Hara, K., 1988, Fluid flow and volume loss during mylonitization: an origin for phyllonite in an overthrust setting, North Carolina, U.S.A., Tectonophysics, v. 156, p. 21-36.

O'Hara, K., and Blackburn, W.H., 1989, Volume-loss model for trace-element enrichments in mylonites, Geology, v. 17, p. 524-527.

Paterson, S.R., and Fowler, T.K., 1993a, Re-examining pluton emplacement processes, Journal of Structural Geology, v. 15, p. 191-206.

Paterson, S.R., and Fowler, T.K., 1993b, Extensional pluton-emplacement models: Do they work for large plutonic complexes?, Geology, v. 21, p. 781-784.

Paterson, S.R., Fowler, T.K., and Miller, R.B., 1996, Pluton emplacement in arcs: a crustal-scale exchange process, Transactions of the Royal Society of Edinburgh: Earth Sciences, v. 87, p. 105-114.

Paterson, S.R., Vernon, R.H., and Fowler, T.K., 1991, Aureole tectonics in Kerrick, D.M., ed., Contact Metamorphism: Mineralogical Society of America Review of Mineralogy, v. 26, p. 673-722.

Presnell, R.D., 1997, Structural controls on the plutonism and metallogeny in the Wasatch and Oquirrh Mountains, Utah in John, D.A., and Ballantyne, G.H., eds., Geology and Ore Deposits of the Oquirrh and Wasatch Mountains, Utah, Society of Economic Geologists Guidebook Series, v. 29, p. 1-14.

Ramsay, J.G., 1989, Emplacement kinematics of a granite diapir: the Chindamora batholith, Zimbabwe, Journal of Structural Geology, v. 11, p. 191-209.

Ramsay, J.G., and Huber, M.I., 1987, *The Techniques of Modern Structural Geology, Volume 2: Folds and Fractures*, Academic Press, 391 pp.

Ramsay, J.G., and Huber, M.I., 1983, *The Techniques of Modern Structural Geology, Volume 1: Strain Analysis*, Academic Press, 307 pp.

Skjernaa, L., 1989, Tubular folds and sheath folds: definitions and conceptual models for their development, with examples from the Grapesvare area, northern Sweden, Journal of Structural Geology, v. 11, p. 689-703.

Simpson, C., 1983, Strain and shape-fabric variations associated with ductile shear zones, Journal of Structural Geology, v. 5, p. 61-72.

Simpson, C., 1986, Determination of movement sense in mylonites, Journal of Geological Education, v. 34, p. 246-261.

Simpson, C., and Schmid, S.M., 1983, An evaluation of criteria to deduce the sense of movement in sheared rocks, Geological Society of America Bulletin, v. 94, p. 1281-1288.

Steinsund, P.I., 1995. StereoNet Version 3.0 for Windows, Geological Software, Tromso, Norway.

Tullis, J., Snoke, A.W., and Todd, V.R., 1982, Penrose Conference report: Significance and petrogenesis of mylonitic rocks, Geology, 10, 227-230

van der Pluijm, B.A., and Marshak, S., 1997, *Earth Structure: An Introduction to Structural Geology and Tectonics*, WCB McGraw-Hill, 495 pp.

Vogel, T.A., Cambray, F.W., Feher, L., Constenius, K.N., and the WIB Research Team, 1997, Petrochemistry and Emplacement History of the Wasatch Intrusive Belt *in* John, D.A., and Ballantyne, G.H., eds., Geology and Ore Deposits of the Oquirrh and Wasatch Mountains, Utah, Society of Economic Geologists Guidebook Series, v. 29, p. 47-63.

Wernic

White,

Willian

Wise, I

Wernicke, B., 1992, Cenozoic extensional tectonics of the U.S. Cordillera in Burchfiel, B.C., Lipman, P.W., and Zoback, M.L., eds., The Cordilleran Orogen: Conterminous U.S., Geological Society of America, Geology of North America, v. G-3, p. 553-581.

White, S.H., Burrows, S.E., Carreras, J., Shaw, N.D., and Humphreys, F.J., 1980, On mylonites in ductile shear zones, Journal of Structural Geology, v. 2, p. 175-187.

Williams, G.D., and Chapman, T.J., 1979, The geometrical classification of noncylindrical folds, Journal of Structural Geology, v. 3, p. 181-185.

Wise, D.U., Dunn, D.E., Engelder, J.T., Geiser, P.A., Hatcher, R.D., Kish, S.A., Odom, A.L., Schamel, S., 1984, Fault-related rocks: suggestions for terminology, Geology, v. 12, p. 391-394.